Preparation of Near-Infrared Emissive π-Conjugated Polymer Films Based on Boron-Fused Azobenzene Complexes with Perpendicularly Protruded Aryl Substituents

Masayuki Gon, Junko Wakabayashi, Masashi Nakamura, Kazuo Tanaka and Yoshiki Chujo*

Department of Polymer Chemistry, Graduate School of Engineering, Kyoto University Katsura, Nishikyo-ku, Kyoto 615-8510, Japan

E-mail: tanaka@poly.synchem.kyoto-u.ac.jp

Key words: boron; conjugated polymer; NIR; solid-state emission; azobenzene

Abstract

Most of organic luminescent dyes usually show poor emission in solid due to aggregation-cause quenching (ACQ) caused by non-specific intermolecular interaction, such as π–π stacking. Furthermore, since commodity molecules having near-infrared (NIR) emission properties tend to have extended π-conjugated systems, development of luminescent organic materials with solid-state NIR emission has been still challenging. Herein, we synthesized the series of the azobenzene complexes with the perpendicularly-protruded aryl derivative at the boron atom toward π-conjugated system. From the optical measurements, it was shown that these complexes can show crystallization-induced emission enhancement (CIEE) behaviors. We also synthesized the donor–acceptor (D–A) type π-conjugated polymers composed of the azobenzene complexes. We obtained highly-efficient NIR emission from the phenyl-substituted polymers both in solution (λ_{PL} = 742 nm, Φ_{PL} = 15%) and film states (λ_{PL} = 793 nm, Φ_{PL} = 9%). Furthermore, emission wavelengths can be tuned by changing the substituent at the boron atom to the modified aryl groups. From mechanistic studies including theoretical calculations, it was shown that electronic interaction is allowable between the aryl substituent to the π-conjugated system through the tetradentate boron.

1. Introduction

Solid-state emission is essential for realizing luminescent devices, such as organic light emitting devices (OLEDs)[1] and luminescent chemical sensors.[2,3] In particular, organic-based π-conjugated polymers received much attention owing to good material properties, such as lightness, processability and flexibility as well as electronic properties, such as luminescence, conductivity and property tunability by chemical modification.[4,5] In particular, because of permeability in various media, near-infrared (NIR) light is utilized for night vision camera, optical communication, identification of target materials and bioimaging.[6–8] Since π-conjugated polymers have a suitable structure for realizing a narrow energy gap which is the origin to generate NIR emission, a wide variety of conjugated polymers with emission in the NIR region have been developed.[9–20] Moreover, by the combination with strong donor and acceptor units, luminescent polymers have been also obtained. However, it is still challenging to obtain NIR emission in film.[8]

Non-specific intermolecular interactions often lead to loss of excited energy through transport the exciton among π–π interaction.[21] This emission annihilation in solid is called as aggregation-caused quenching (ACQ) or concentration quenching. To improve device efficiency in OLEDs and robust luminescent bioprobes for quantitative analyses, elaborate molecular structures for avoiding ACQ are needed.[22–24] Insulated molecular wires (IMWs) are known to be one of sophisticated ideas for obtaining solid-state emission.[25] By wrapping each π-conjugated main chain with bulky substituents at the side chains, intermolecular interactions are inhibited. As a result, emission properties in the diluted solution can be preserved in the condensed state. Following this concept, bright emissive π-conjugated polymers have been developed.[26–

[29] However, the complicated synthetic processes are required for applying this concept to extended π-conjugated systems which are capable of presenting NIR luminescence. As another strategy, the class of molecules having aggregation-induced emission (AIE) or crystallized-induced emission enhancement (CIEE) properties, which show emission only in solid or emission enhancement in crystal, respectively, have recently attracted attention.[30–32] Simply by using AIE- and/or CIEE molecules as a monomer, solid-state luminescent polymers have been obtained.[33–38] However, most of AIE molecules have twisted molecular structures for inhibiting intermolecular interactions in aggregation, and extension of π-electron delocalization should be also disturbed. Therefore, in principle, it is difficult to apply conventional AIE molecules as a monomer for obtaining narrow-energy-gap polymers.

Recently, we have proposed the design concept based on “element-blocks” which is a minimum functional unit containing heteroatoms.[39–41] By employing unique properties of heteroatoms, various types of luminescent dyes and polymers have been developed.[42–54] As a luminescent “element-block”, we focused on the complexes having a tetracoordinated boron atom.[55] Boron complexation has been used for reinforcing molecular rigidity and planarity. Because these structural features are suitable for extending π-conjugation, a huge number of luminescent complexes, such as boron dipyrromethene (BODIPY), have been developed.[56] However, due to high planarity of these complexes, non-specific intermolecular interactions such as π–π stacking, followed by excitation decay, critically occurs in condensed states. Therefore, we usually suffer from ACQ for obtaining solid-state luminescent materials. Meanwhile, we found boron ketoiminate and boron diiminate complexes exhibited AIE and CIEE properties which are promising characters for creating solid-state emissive materials.[57–

[67] More recently, the tetracoordinated boron complexes with azomethine and azobenzene-based tridentate ligands were found to show AIE and CIEE in deep red regions.[68–74] From the mechanistic studies, it is proposed that π-conjugated system can be well expanded through whole molecules although the structures of these complexes are slightly bent. Furthermore, the perpendicularly-protruded fluorine substituents at the boron atom toward main-chain conjugation should disturb intermolecular interaction in the crystalline state.[68,71,72] From these results, we presumed that much narrower band gaps and more intense solid-state luminescence could be realized in the azobenzene complex.

From this standpoint, we focused on unique chemical conformation of the tetracoordinated boron. It is presumed that introduction of a bulky substituent on boron is expected to inhibit non-specific π–π interaction in the condensed state owing to the perpendicularly-protruded geometry against π-surface. To evaluate validity of this idea and to accomplish NIR emission especially in solid by suppressing ACQ, we designed the boron complexes with the azobenzene tridentate ligand, which is capable of working as a strong acceptor by combining boron atom,[72–74] having the aryl substituents at the boron atom. Herein, we report syntheses and optical properties of the series of the complexes and polymers containing the modified azobenzene structures. We found that these materials can show efficient NIR emission. In particular, emission properties can be tuned by the substituent effect at the boron atom. From theoretical and kinetic investigations, we discuss the roles of the substituents. We demonstrate the simple and effective design strategy utilizing the feature of heteroatom for constructing bright-emissive π-conjugated polymers.

2.1 Synthesis

Scheme 1 shows the synthesis of the boron-fused complexes with various aryl groups at the boron atom (**BAz-C6F5**, **BAz-Ph** and **BAz-Mes**). The ligand, 6,6′-(diazene-1,2-diyl)bis(3-bromophenol) (**L-Az**), was prepared according to the previous report.[72] The complex **BAz-C6F5** was synthesized by the condensation reaction between **L-Az** and 2,3,4,5,6-pentafluorophenylboronic acid ($C_6F_5B(OH)_2$) in acetonitrile under reflux condition for 72 h in 43% isolated yield. The mixture of **L-Az** and dichlorophenylborane ($PhBCl_2$) in toluene and Et_3N was reacted at 100 °C for 24 h, then the target complex **BAz-Ph** was obtained in 44% isolated yield. **BAz-Mes** was also synthesized from **L-Az** and dimesitylfluoroborane (Mes_2BF) by the same manner with **BAz-Ph** in 43% isolated yield. **BAz-F** was also prepared according to the literature for comparison.[72] Next, by using the obtained boron-fused azobenzene (**BAz**) complexes as a monomer, electron donor–acceptor (D–A) type π-conjugated copolymers with a bithiophene co-monomer were prepared (**Scheme 2** and **Table 1**). Migita–Kosugi–Stille cross-coupling polymerizations[75,76] with **BAz-C6F5**, **BAz-Ph** or **BAz-Mes** and 5,5′-bis(trimethylstannyl)-3,3′-didodecyl-2,2′-bithiophene (**BT**) were executed in a catalytic system involving $Pd_2(dba)_3$ (dba = dibenzylideneacetone) and 2-dicyclohexylphosphino-2′,4′,6′-triisopropylbiphenyl (XPhos) to afford a copolymer **P-BAz-C6F5**, **P-BAz-Ph**, **P-BAz-Mes**, respectively. The synthetic results and polymer data are listed in **Table 1**. In this research, the data from **P-BAz-F** in our previous work is also cited as comparison.[72] All synthesized compounds showed good solubility in common organic solvents such as toluene, chloroform, dichloromethane and tetrahydrofuran (THF) and can be characterized by ^{1}H, ^{13}C, ^{11}B NMR, MS spectra (see

Supporting Information). From these characterization data, we concluded that the samples have the desired structures and enough purity for further analyses.

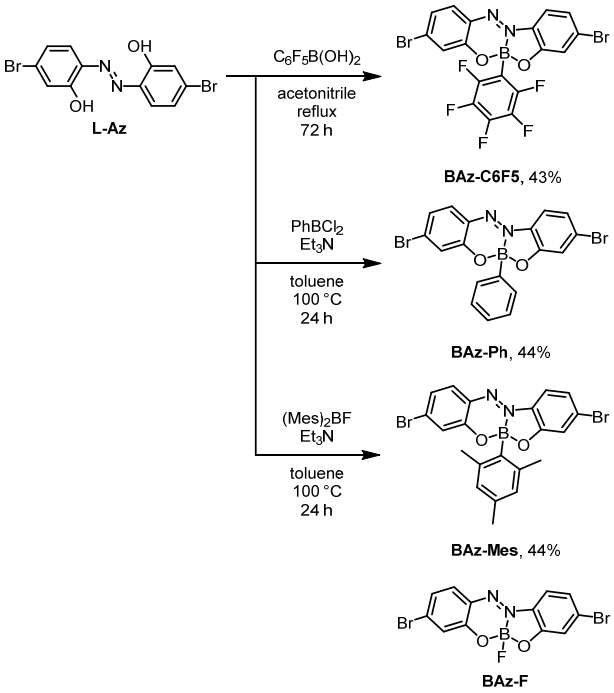

Scheme 1. Syntheses of monomers, **BAz-C6F5**, **BAz-Ph** and **BAz-Mes**, and chemical structure of **BAz-F**.

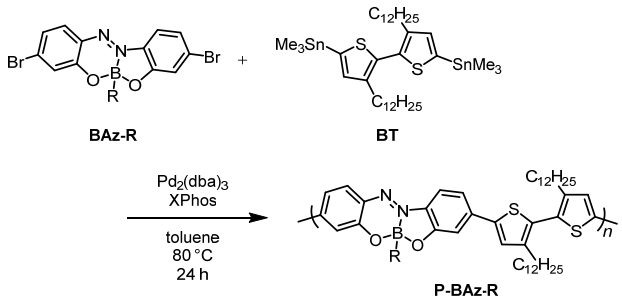

Scheme 2. General procedure for preparing polymers, **P-BAz-C6F5**, **P-BAz-Ph** and **P-BAz-Mes**.

Table 1. Molecular weights and reaction yields of the synthesized polymers

	R	M_n[a] /kDa	M_w[a] /kDa	M_w/M_n	yield /%
P-BAz-F[b]	F	21.4	55.6	2.5	85
P-BAz-C6F5	C_6F_5	15.9	39.1	2.5	95
P-BAz-Ph	Ph	13.8	29.8	2.2	94
P-BAz-Mes	Mes	17.1	45.1	2.6	86

[a] Determined by a gel permeation chromatography (GPC) with polystyrene standards
[b] ref 72.

2.2 Optical measurements

To examine the substituent effect on the electronic structures in the ground state, UV–vis absorption measurements (1.0×10^{-5} M) were carried out in toluene (**Figures 1**, **2A**, **S1** and **Table 2**). The order of the wavelengths of absorption maxima (λ_{abs}) of the **BAz** complexes seems to be correlated with the type of the substituent at the boron atom. By increasing electron-donating ability, the bathochromic effect on the peak wavelength was observed, meaning that narrower energy gaps are inducible by the electron-donating substituent effect, similarly to conventional conjugated systems. It

should be noted that the perpendicularly-protruded substituent at the boron atom is able to perturb the electronic properties of the **BAz** complexes in the ground state.

The polymers exhibited their absorption bands in the longer wavelength regions than those of the corresponding monomers. It is likely that strong electronic D–A interaction through polymer chains involving the N=N double bonds with the bithiophene units should contribute to red-shifted absorption spectra.[72] Moreover, as observed in the monomers, it was shown that the electron-donating ability of the substituent at the boron atom seems to be responsible for the bathochromic shift of the absorption bands, meaning that the substituent effect is applicable for tuning electronic properties of main-chain conjugation. Homogeneous thin films were able to be easily prepared with the commodity spin-coated method owing to good film-formability of the synthesized polymers. In **Figure 2B** and **Table 3**, the slight bathochromic shifts and broader absorption bands were observed from the film samples compared to those in the diluted solutions. The aryl derivative-substituted polymers provided narrower spectra than **P-BAz-F**, implying that the bulky substituents might be favorable for suppressing intermolecular interaction between polymer chains even in the condensed state.

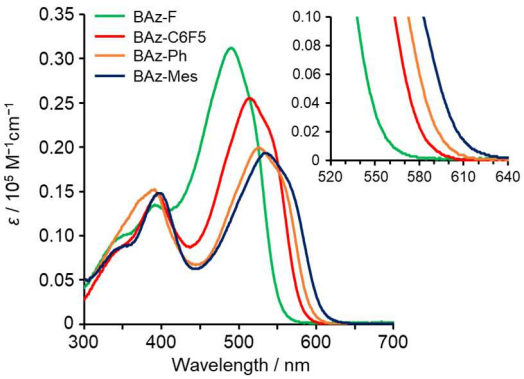

Figure 1. UV–vis absorption spectra of the **BAz** complexes in toluene (1.0×10^{-5} M). The inserted chart denotes enlarged view at edge of the spectra for estimation of optical band gaps.

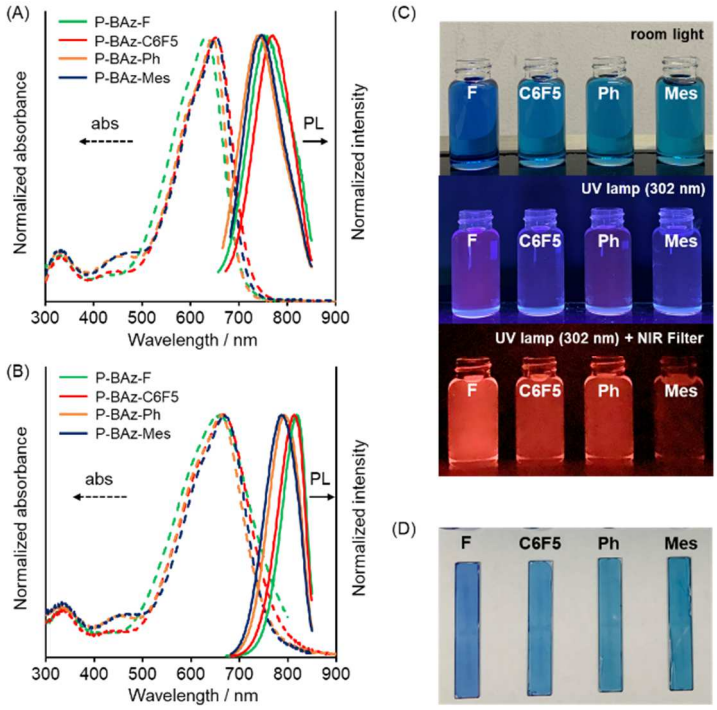

Figure 2. UV–vis absorption (dotted line) and PL spectra (solid line) of the **BAz** polymers (A) in toluene (1.0×10^{-5} M per repeating unit) and (B) in film with the excitation light at each absorption maximum. (C) Photos of the **BAz** polymers in toluene (NIR filter cuts the light under 700 nm) and (D) in film.

Table 2. Optical data of the **BAz** monomers and polymers in toluene

	λ_{abs}[a] /nm	λ_{PL}[a] /nm	Φ_{PL}[a,b] /%	τ[a,c] (α) /ns	k_r[d] /$10^8 s^{-1}$	k_{nr}[d] /$10^8 s^{-1}$
BAz-F	490	616	<1	–[e]	–[e]	–[e]
BAz-C6F5	514	628	<1	–[e]	–[e]	–[e]
BAz-Ph	526	635	<1	–[e]	–[e]	–[e]
BAz-Mes	535	651	<1	–[e]	–[e]	–[e]
P-BAz-F	632	751	25	0.68	3.7	11
P-BAz-C6F5	651	767	14	0.38 (80%)	3.0	18
				0.67 (20%)		
P-BAz-Ph	646	742	15	0.27 (75%)	4.3	24
				0.49 (25%)		
P-BAz-Mes	653	736	4	0.13 (94%)	1.7	46
				0.52 (6%)		

[a] 1.0×10^{-5} M for monomers and 1.0×10^{-5} M per repeating unit for polymers; excited at absorption maxima for PL.

[b] Absolute PL quantum yield excited at absorption maxima.

[c] Emission lifetime at λ_{PL}.

[d] $k_r = \Phi_{PL}/\tau_{av}$, $k_{nr} = (1 - \Phi_{PL})/\tau_{av}$, $\tau_{av} = \Sigma\alpha_i\tau_i^2/\Sigma\alpha_i\tau_i$, α: relative amplitude.

[e] Not detected.

Table 3. Optical data of **BAz** monomers and polymers in solid state

	λ_{abs}[a] /nm	λ_{PL}[a] /nm	Φ_{PL}[a,b] /%	τ[a,c] (α) /ns	k_r[d] /$10^8 s^{-1}$	k_{nr}[d] /$10^8 s^{-1}$
BAz-F	–[e]	652	8	0.74	1.1	13
BAz-C6F5	–[e]	644	7	0.66 (14%)	0.48	6.5
				1.5 (86%)		
BAz-Ph	–[e]	659	12	0.58 (3%)	0.35	2.6
				3.4 (97%)		
BAz-Mes	–[e]	662	2	0.26 (77%)	0.45	28
				0.52 (23%)		
P-BAz-F	661	818	4	–[e]	–[e]	–[e]
P-BAz-C6F5	665	814	6	–[e]	–[e]	–[e]
P-BAz-Ph	662	793	9	–[e]	–[e]	–[e]
P-BAz-Mes	668	787	5	–[e]	–[e]	–[e]

[a] Solid state for monomers and spin-coated film on the quartz substrate (0.9 cm×5 cm) prepared from chloroform solution (0.10 mL, 1000 rpm, concentration: 1.0 mg/0.30 mL) for polymers; excited at absorption maxima for PL.

[b] Absolute PL quantum yield excited at absorption maxima.

[c] Emission lifetime at λ_{PL}.

[d] $k_r = \Phi_{PL}/\tau_{av}$, $k_{nr} = (1-\Phi_{PL})/\tau_{av}$, $\tau_{av} = \Sigma\alpha_i\tau_i^2/\Sigma\alpha_i\tau_i$, α: relative amplitude.

[e] Not detected.

To evaluate electronic structures of the **BAz** complexes in the excited state, the photoluminescence (PL) properties were evaluated in toluene (1.0×10^{-5} M, **Figure S2**) and crystal. It was clearly demonstrated that CIEE properties were obtained from the complexes (**Table 3**). The emission intensity was obviously very weak in solution (Φ_{PL} < 1%), whereas intense emission was observed in crystal (**Figure 3**). According to the previous work, the critical emission quenching in solution should be caused by excitation-driven bending motions as shown in the series of tetracoordinated boron with the tridentate ligand.[68,72,77] These molecular motions, which are promised to induce excitation decay, would be effectively suppressed by structural restriction in crystal packing. Furthermore, the perpendicularly-protruded substituents should play significant roles in inhibition of intermolecular interaction in the condensed state. [68,71,72] Consequently, CIEE properties should be obtained from the **BAz** complexes. For obtaining information on the mechanism, we calculated a radiative rate constant (k_r) and a non-radiative rate constant (k_{nr}) from the PL lifetime measurements (**Figure S3** and **Table 3**). Due to low emission intensity in solution, the kinetic data were obtained only in the solid state. The aryl substituents tend to exhibit lower k_{nr} values in comparison to **BAz-F**. It is probably because intermolecular interaction should be disturbed by the bulky substituents. The larger k_{nr} value of **BAz-Mes** implies that molecular tumbling at the methyl substituents might promote non-radiative deactivation pathways. The simple and bulky structure of the phenyl group is favorable for the presavation of the excited state (τ = 3.4 ns). The unusual large k_r value was obtained from **BAz-F**, and the similar extraordinal rapid process was also detected in the crystalline sample of the boron azomethine complex where one of nitrogens in the azobenzene skeleton is replaced to carbon.[68,71] Tight packing might contribute to accelating radiative decay processes

followed by emission enhancment in crystal.

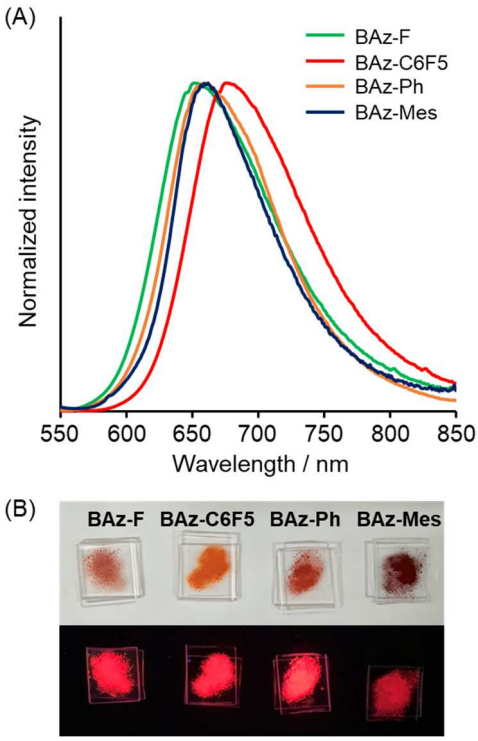

Figure 3. (A) PL spectra of **BAz** complexes in solid with the excitation light at each absorption maximum detected in toluene. (B) Photos of the solid samples under room light (upper) and UV irradiation (365 nm).

In contrast to the environment-sensitive luminescent behaviors of the monomers, intense NIR emission was obtained from the polymers in the solution state (**Figure 2A** and **Table 2**). According to the λ_{PL}s and Φ_{PL}s of the synthesized polymers, it can be said that the **BAz** skeleton should be the versatile π-conjugated scaffold for constructing NIR-emissive "element-blocks". By incorporating the complexes into the polymer chains, the excitation-driven molecular motions would be prohibited.[72,77] As a result, emission should be induced in solution. Significant enhancement of k_r ($>10^8$ s^{-1}) was achieved by the expansion of π-conjugation and formation of D–A interaction with the bithiophene units. Lager k_{nr} values of the **BAz** polymers with the aryl substituents were observed. Intramolecular skeletal bending can be prohibited by the polymerization, while molecular motions at the substituents at the boron atom occur and activate non-radiative decay channels.

In the films, the **BAz** polymers exhibited intense emission (**Figure 2B** and **Table 3**). It should be emphasized that the emission peak wavelengths were drastically varied by changing the type of the substituents without critical losses of emission efficiencies. From 787 nm to 818 nm, peak positions were altered, representing that the perpendicular-protruded substituents significantly affect electronic structures of the polymer conjugations in the excited state. By suppressing molecular motions including intramolecular bending and tumbling at the substituent as well as intramolecular interactions by the substituent at the boron atoms, solid-state NIR emission with relatively-larger emission efficiency can be obtained. In the case of **P-BAz-F**, larger degree of ACQ was observed with the peak position in the longer wavelength region than those of the others. Intermolecular interaction among polymer chains could occur

in film and self-absorption caused by the broader absorption band should sharpen the PL spectrum. This result proposes that the aryl substituents could be advantageous for preserving emission properties in the condensed state. By employing the azobenzene structure with the aryl substituents, not only suppression of ACQ but also tuning of luminescent wavelengths in the NIR region can be demonstrated.

2.3 Cyclic voltammetry

To collect further information on the substituent effect, we evaluated energy levels with cyclic voltammetry (CV). The results are shown in **Figure 4** and **Table 4**. The LUMO energy levels were estimated from the onset of the reduction curve. In both of **BAz** monomers and polymers, it was found that LUMO energy levels were affected by the inductive effect of substituents at the boron atom. The higher electron-accepting ability of **BAz-C6F5** and the lower ones of **BAz-Ph** and **BAz-Mes** were good agreement with the order of λ_{PL} of the D–A polymers. In other words, the low-lying LUMO energy level constructed strong charge transfer (CT) state. In **BAz** monomers, the HOMO energy levels were not able to be estimated from the cyclic voltammograms because oxidation peaks were out of the potential window. Instead, we calculated the HOMO energy levels using optical band gaps ($E_{g,opt}$) obtained from the UV–vis absorption spectra. Accordingly, it was shown that the HOMO energy levels were elevated by the electron-donating substituents. In summary, it was confirmed that energy levels of frontier orbitals can be tuned by the substituent effect at the boron atom.

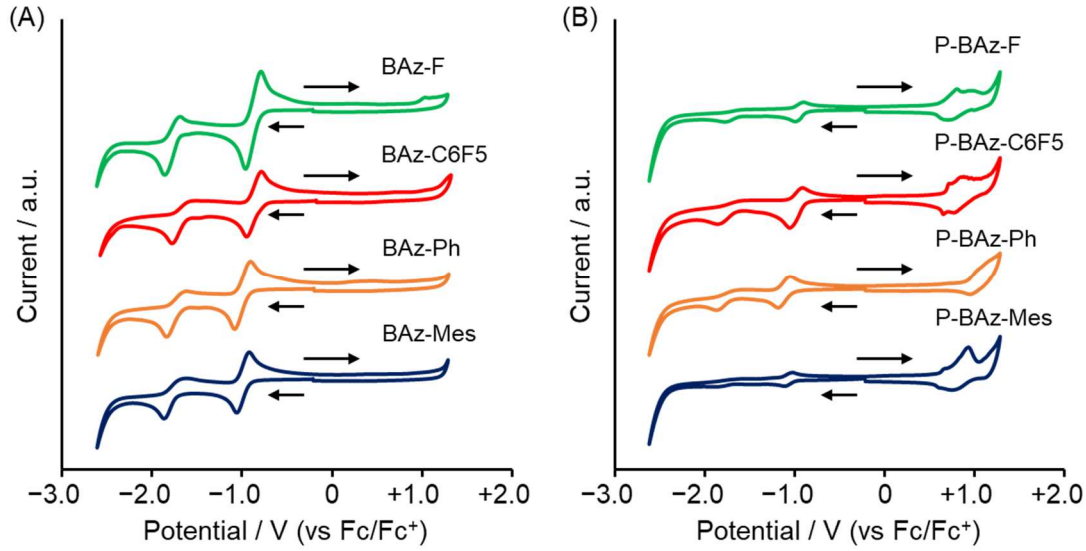

Figure 4. Cyclic voltammograms of (A) **BAz** monomers and (B) **BAz** polymers in dichloromethane (1.0×10^{-3} M for monomers, 1.0×10^{-3} M per repeating unit for polymers) containing nBu$_4$NPF$_6$ (0.10 M) at room temperature with a scan rate of 0.1 V s^{-1}. The black arrows denote sweep directions.

Table 4. Energy levels of molecular orbitals of **BAz** complexes

	$\lambda_{abs,edge}$ [a] /nm	$E_{g,opt}$ [b] /eV	E_{onset}^{red} [c] /V	E_{LUMO} [d] /eV	E_{HOMO} [d] /eV
BAz-F	550	2.25	−0.80	−4.00	−6.25
BAz-C6F5	579	2.14	−0.79	−4.01	−6.15
BAz-Ph	592	2.09	−0.91	−3.89	−5.98
BAz-Mes	606	2.05	−0.92	−3.88	−5.93
P-BAz-F	700	1.77	−0.86	−3.94	−5.71
P-BAz-C6F5	721	1.72	−0.88	−3.92	−5.64
P-BAz-Ph	699	1.77	−1.01	−3.79	−5.57
P-BAz-Mes	711	1.74	−0.98	−3.82	−5.56

[a] In toluene (1.0×10^{-5} M for monomers, 1.0×10^{-5} M per repeating unit for polymers), estimated from **Figure 1** and **Figure S1**.

[b] $E_{g,opt} = 1240/\lambda_{abs,edge}$.

[c] In dichloromethane (1.0×10^{-3} M for monomers, 1.0×10^{-3} M per repeating unit for polymers) containing nBu$_4$NPF$_6$ (0.10 M) at room temperature with a scan rate of 0.1 V s^{-1}.

[d] $E_{LUMO} = -(4.8-E_{onset}^{red})$ (eV),[78,79] $E_{HOMO} = E_{LUMO}-E_{g,opt}$.

2.4 Theoretical calculation

Theoretical calculation with density functional theory (DFT) at B3LYP/6-311G(d,p) level was performed to support experimental results. The results are shown in **Figure 5**. The tendency of calculated HOMO and LUMO energy levels and the energy gaps of allowed transition bands were almost good agreements with the results from optical and electrochemical measurements (**Figures 5A** and **5B**). The electronic distribution at the aryl substituents was clearly observed in HOMOs, especially in **BAz-Ph** and **BAz-Mes** (**Figure 5C**). These data can strongly support the experimental results that the perpendicularly-protruded aryl groups are capable of perturbing electronic structures of the main-chain conjugation. To estimate influence on the electronic structures in polymers, the model compounds modified with the **BT** units in both sides of **BAz** complexes were used for calculations (**Figures 6**, **S5** and **Table S1**). Slight MO distribution was observed in HOMO, meaning that electronic structures at the **BAz** complex should be sensitive to the connecting molecules. It is shown that optical properties of the **BAz** polymers can be tuned by selecting the substituent at the boron atom as well as the comonomer.

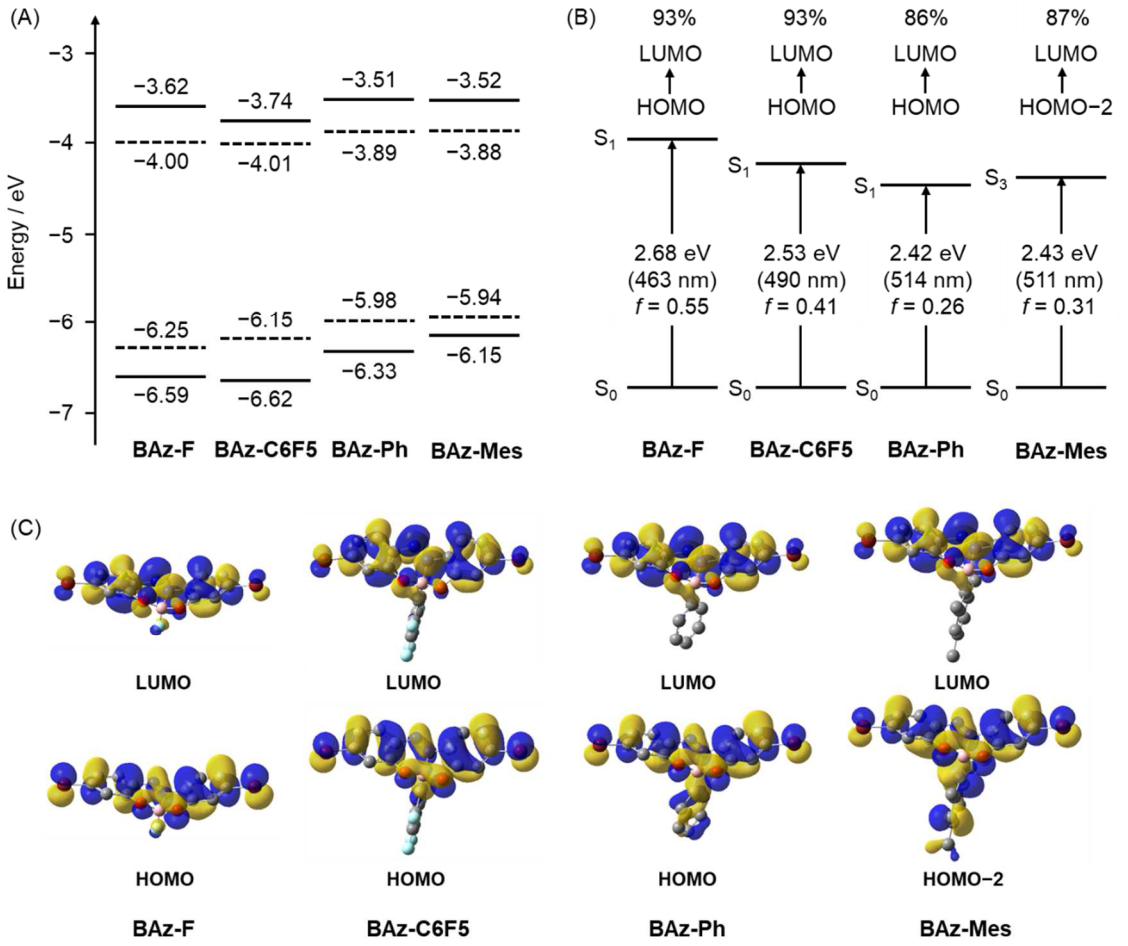

Figure 5. (A) Energy diagrams (solid line: from DFT calculation, dotted line: from CV and UV–vis absorption spectra, **Table 4**), (B) allowed transition bands and main contributed MOs with rate of contribution (*f*: oscillator strength), and (C) selected Kohn–Sham orbitals of **BAz** complexes obtained from DFT or TD-DFT calculations (isovalue = 0.02). Hydrogens were omitted for clarity.

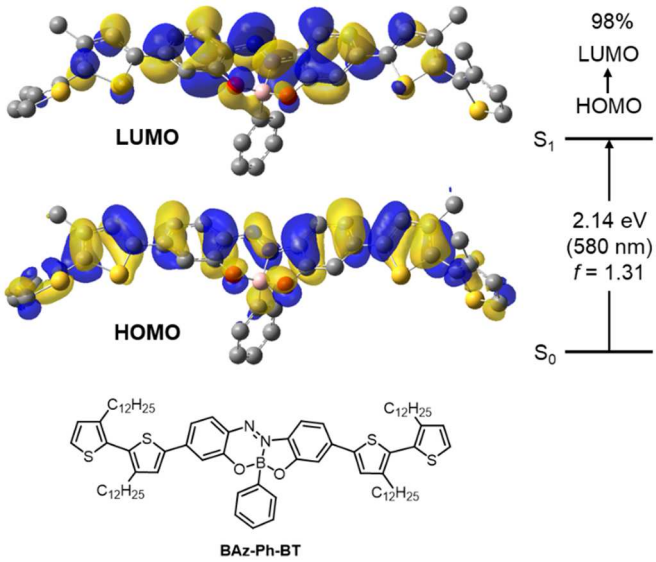

Figure 6. HOMO and LUMO of the model compound **BAz-Ph-BT**, $S_0 \rightarrow S_1$ transition band and main contributed MOs with rate of contribution (*f*: oscillator strength) obtained with DFT or TD-DFT calculations (isovalue = 0.02). Hydrogens were omitted for clarity.

3. Conclusion

The substituent effects at the boron atom in the boron-fused azobenzene (**BAz**) complexes were investigated. The π-delocalized electronic interaction by the aryl rings raised HOMO energy levels and induced bathochromic shifts of absorption bands. The synthesized **BAz** complexes showed CIEE properties. Finally, we obtained solid-state NIR-luminescent polymers including the **BAz** complex modified with the aryl substituents. In the molecular design for deep-red and NIR luminescent polymers, extension of π-conjugation and/or incorporation of strong electron donor and acceptor into the extended π-conjugated systems are conventional. In contrast, we demonstrate here that the perpendicular-protruded aryl groups can perturb electronic conjugation not only in the azobenzene ligand but also in the conjugated polymers. Moreover, owing to steric hindrance, solid-state luminescence is inducible in solid and film by suppressing intermolecular interactions followed by ACQ. We think that new intrinsic characters of the tetracoordinated born can be revealed in this study.

Supporting Information

Supporting Information is available from the Wiley Online Library or from the author.

Acknowledgements

This work was partially supported by the Mizuho Foundation for the Promotion of Sciences, Japan (for M.G.) and a Grant-in-Aid for Early-Career Scientists (for M.G.) (JSPS KAKENHI Grant numbers 20K15334), for Scientific Research (B) (for K.T), (JP17H03067), for Scientific Research on Innovative Areas “New Polymeric Materials

Based on Element-Blocks (No.2401)" (JP24102013) and for Challenging Research (Pioneering) (JP18H05356).

References

[1] Y. Watanabe, H. Sasabe, J. Kido, *Bull. Chem. Soc. Jpn.* **2019**, *92*, 716.

[2] W. Guan, W. Zhou, J. Lu, C. Lu, *Chem. Soc. Rev.* **2015**, *44*, 6981.

[3] W. T. Samuel, D. J. Guy and M. S. Timothy, *Chem. Rev.*, **2007**, 4, 1339.

[4] A. Pron, P. Rannou, *Prog. Polym. Sci.* **2002**, *27*, 135.

[5] S. E. Root, S. Savagatrup, A. D. Printz, D. Rodriquez, D. J. Lipomi, *Chem. Rev.* **2017**, *117*, 6467.

[6] H. Xiang, J. Cheng, X. Ma, X. Zhou, J. J. Chruma, *Chem. Soc. Rev.* **2013**, *42*, 6128.

[7] L. Yuan, W. Lin, K. Zheng, L. He, W. Huang, *Chem. Soc. Rev.* **2013**, *42*, 622.

[8] A. Zampetti, A. Minotto, F. Cacialli, *Adv. Funct. Mater.* **2019**, *29*, 1807623.

[9] N. Suzuki, M. Wakioka, F. Ozawa, S. Yamaguchi, *Asian J. Org. Chem.* **2020**, *9*, 1326.

[10] J. Liu, J. Geng, B. Liu, *Chem. Commun.* **2013**, *49*, 1491.

[11] S. Wang, J. Liu, G. Feng, L. G. Ng, B. Liu, *Adv. Funct. Mater.* **2019**, *29*, 1808365.

[12] C. Rohatgi, T. Harada, E. F. Need, M. Krasowska, D. A. Beattie, G. D. Dickenson, T. A. Smith, T. W. Kee, *ACS Appl. Nano Mater.* **2018**, *1*, 4801.

[13] L. Chen, D. Chen, Y. Jiang, J. Zhang, J. Yu, C. C. DuFort, S. R. Hingorani, X. Zhang, C. Wu, D. T. Chiu, *Angew. Chem. Int. Ed.* **2019**, *58*, 7008.

[14] G. Deng, X. Peng, Z. Sun, W. Zheng, J. Yu, L. Du, H. Chen, P. Gong, P. Zhang, L. Cai, B. Z. Tang, *ACS Nano* **2020**, *14*, 11452.

[15] P. R. Neumann, D. L. Crossley, M. Turner, M. Ingleson, M. Green, J. Rao, L. A. Dailey, *ACS Appl. Mater. Interfaces* **2019**, *11*, 46525.

[16] X. Ma, X. Jiang, S. Zhang, X. Huang, Y. Cheng, C. Zhu, *Polym. Chem.* **2013**, *4*, 4396.

[17] H.-Y. Liu, P.-J. Wu, S.-Y. Kuo, C.-P. Chen, E.-H. Chang, C.-Y. Wu, Y.-H. Chan, *J. Am. Chem. Soc.* **2015**, *137*, 10420.

[18] X. Li, W. Zeng, Y. Zhang, Q. Hou, W. Yang, Y. Cao, *Eur. Polym. J.* **2005**, *41*, 2923.

[19] R. Yoshii, A. Nagai, Y. Chujo, *J. Polym. Sci. A Polym. Chem.* **2010**, *48*, 5348.

[20] R. Yoshii, A. Nagai, K. Tanaka, Y. Chujo, *J. Polym. Sci. A Polym. Chem.* **2013**, *51*, 1726.

[21] S. A. Jenekhe and J. A. Osaheni, *Science* **1994**, 265, 765.

[22] T. Sato, D.-L. Jiang, T. Aida, *J. Am. Chem. Soc.* **1999**, 121, 10658.

[23] C.-H. Zhao, A. Wakamiya, S. Yamaguchi, *Macromolecules* **2007**, 40, 3898.

[24] J. Bouffard, T. M. Swager, *Macromolecules* **2008**, 41, 5559.

[25] M. J. Frampton, H. L. Anderson, *Angew. Chem. Int. Ed.* **2007**, *46*, 1028-1064.

[26] F. Cacialli, J. S. Wilson, J. J. Michels, C. Daniel, C. Silva, R. H. Friend, N. Severin, P. Samorì, J. P. Rabe, M. J. O'Connell, P. N. Taylor, H. L. Anderson, *Nat. Mater.* **2002**, *1*, 160.

[27] C. Pan, K. Sugiyasu, Y. Wakayama, A. Sato, M. Takeuchi, *Angew. Chem. Int. Ed.* **2013**, 52, 10775.

[28] T. Hosomi, H. Masai, T. Fujihara, Y. Tsuji, J. Terao, *Angew. Chem. Int. Ed.* **2016**, 55, 13427.

[29] A. Leventis, J. Royakkers, A. G. Rapidis, N. Goodeal, M. K. Corpinot, J. M. Frost, D.-K. Bučar, M. O. Blunt, F. Cacialli, H. Bronstein, *J. Am. Chem. Soc.* **2018**, *140*, 1622.

[30] J. Mei, N. L. C. Leung, R. T. K. Kwok, J. W. Y. Lam, B. Z. Tang, *Chem. Rev.* **2015**, *115*, 11718.

[31] J. Luo, Z. Xie, J. W. Y. Lam, L. Cheng, H. Chen, C. Qiu, H. S. Kwok, X. Zhan, Y. Liu, D. Zhu, B. Z. Tang, *Chem. Commun.* **2001**, 1740.

[32] Y. Dong, J. W. Y. Lam, A. Qin, Z. Li, J. Sun, H. H.-Y. Sung, I. D. Williams, B. Z. Tang, *Chem. Commun.* **2007**, 40.

[33] R. Hu, J. L. Maldonado, M. Rodriguez, C. Deng, C. K. W. Jim, J. W. Y. Lam, M. M. F. Yuen, G. Ramos-Ortiz, B. Z. Tang, *J. Mater. Chem.* **2012**, *22*, 232.

[34] Z. Qiu, T. Han, R. T. K. Kwok, J. W. Y. Lam, B. Z. Tang, *Macromolecules* **2016**, *49*, 8888.

[35] K. R. Ghosh, S. K. Saha, Z. Y. Wang, *Polym. Chem.* **2014**, *5*, 5638.

[36] S. Dineshkumar, I. R. Laskar, *Polym. Chem.* **2018**, *9*, 5123.

[37] B. R. He, S. H. Ye, Y. J. Guo, B. Chen, X. F. Xu, H. Y. Qiu, Z. J. Zhao, *Sci. China Chem.* **2013**, *56*, 1221.

[38] W. Wu, S. Ye, R. Tang, L. Huang, Q. Li, G. Yu, Y. Liu, J. Qin, Z. Li, *Polymer* **2012**, *53*, 3163.

[39] Y. Chujo, K. Tanaka, *Bull. Chem. Soc. Jpn.* **2015**, *88*, 633.

[40] M. Gon, K. Tanaka, Y. Chujo, *Polym. J.* **2018**, *50*, 109.

[41] K. Tanaka, Y. Chujo, *Polym. J.* **2020**, *52*, 555.

[42] J. Ochi, K. Tanaka, Y. Chujo, *Angew. Chem. Int. Ed.* **2020**, *59*, 9841.

[43] K. Nishino, K. Tanaka, Y. Chujo, *Asian J. Org. Chem.* **2019**, *8*, 2228.

[44] H. Watanabe, Y. Kawano, K. Tanaka, Y. Chujo, *Asian J. Org. Chem.* **2020**, *9*, 259.

[45] M. Yamaguchi, K. Tanaka, Y. Chujo, *Chem. Asian J.* **2018**, *13*, 1342.

[46] S. Ito, A. Hirose, M. Yamaguchi, K. Tanaka, Y. Chujo, *Polymers* **2017**, *9*, 68.

[47] B. Yuan, H. Wang, J.-F. Xu, X. Zhang, *ACS Appl. Mater. Interfaces* **2020**, *12*, 26982.

[48] H. Dang, Y. Li, H. Zou, S. Liu, *Dyes Pigments* **2020**, *172*, 107804.

[49] T. Ono, Y. Tsukiyama, A. Taema, H. Sato, H. Kiyooka, Y. Yamaguchi, A. Nagahashi, M. Nishiyama, Y. Akahama, Y. Ozawa, M. Abe, Y. Hisaeda, *ChemPhotoChem* **2018**, *2*, 416.

[50] M. Shimizu, D. Ryuse, T. Kinoshita, *Chem. Eur. J.* **2017**, *23*, 14623.

[51] H. Imoto, T. Fujii, S. Tanaka, S. Yamamoto, M. Mitsuishi, T. Yumura, K. Naka, *Org. Lett.* **2018**, *20*, 5952.

[52] C. Yamazawa, H. Imoto, K. Naka, *Chem. Lett.* **2018**, *47*, 887.

[53] Y. Sato, Y. Mutoh, D. Matsukuma, M. Nakagawa, T. Kawai, K. Isoda, *Chem. Asian J.* **2018**, *13*, 2619.

[54] Y. Matsumura, H. Nishiyama, S. Inagi, I. Tomita, *J. Polym. Sci. Part A: Polym. Chem.* **2019**, *57*, 2519.

[55] K. Tanaka, Y. Chujo, *Macromol. Rapid Commun.* **2012**, *33*, 1235.

[56] A. Loudet, K. Burgess, *Chem. Rev.* **2007**, *107*, 4891.

[57] R. Yoshii, A. Nagai, K. Tanaka, Y. Chujo, *Chem. Eur. J.* **2013**, *19*, 4506.

[58] R. Yoshii, K. Tanaka, Y. Chujo, *Macromolecules* **2014**, *47*, 2268.

[59] R. Yoshii, K. Suenaga, K. Tanaka, Y. Chujo, *Chem. Eur. J.* **2015**, *21*, 7231.

[60] K. Suenaga, R. Yoshii, K. Tanaka, Y. Chujo, *Macromol. Chem. Phys.* **2016**, *217*, 414.

[61] K. Suenaga, K. Uemura, K. Tanaka, Y. Chujo, *Polym. Chem.* **2020**, *11*, 1127.

[62] R. Yoshii, A. Hirose, K. Tanaka, Y. Chujo, *Chem. Eur. J.* **2014**, *20*, 8320.

[63] R. Yoshii, A. Hirose, K. Tanaka, Y. Chujo, *J. Am. Chem. Soc.* **2014**, *136*, 18131.

[64] S. Ito, A. Hirose, M. Yamaguchi, K. Tanaka, Y. Chujo, *J. Mater. Chem. C* **2016**, *3*, 5564.

[65] M. Yamaguchi, S. Ito, A. Hirose, K. Tanaka, Y. Chujo, *J. Mater. Chem. C* **2016**, *3*, 5314.

[66] M. Yamaguchi, S. Ito, A. Hirose, K. Tanaka, Y. Chujo, *Mater. Chem. Front.* **2017**, *1*, 1573.

[67] M. Yamaguchi, S. Ito, A. Hirose, K. Tanaka, Y. Chujo, *Polym. Chem.* **2018**, *9*, 1942.

[68] S. Ohtani, M. Gon, K. Tanaka, Y. Chujo, *Chem. Eur. J.* **2017**, *23*, 11827.

[69] S. Ohtani, M. Gon, K. Tanaka, Y. Chujo, *Macromolecules* **2019**, *52*, 3387.

[70] S. Ohtani, M. Nakamura, M. Gon, K. Tanaka, Y. Chujo, *Chem. Commun.* **2020**, *56*, 6575.

[71] S. Ohtani, M. Gon, K. Tanaka, Y. Chujo, *Crystals* **2020**, *10*, 615.

[72] M. Gon, K. Tanaka, Y. Chujo, *Angew. Chem. Int. Ed.* **2018**, *57*, 6546.

[73] M. Gon, J. Wakabayashi, K. Tanaka, Y. Chujo, *Chem. Asian J.* **2019**, *14*, 1837.

[74] J. Wakabayashi, M. Gon, K. Tanaka, Y. Chujo, *Macromolecules* **2020**, *53*, 4524.

[75] M. Kosugi, K. Sasazawa, Y. Shimizu, T. Migita, *Chem. Lett.* **1977**, *6*, 301.

[76] D. Milstein, J. K. Stille, *J. Am. Chem. Soc.* **1978**, *100*, 3636.

[77] M. Gon, K. Tanaka, Y. Chujo, *Bull. Chem. Soc. Jpn.* **2019**, *92*, 7.

[78] J. Pommerehne, H. Vestweber, W. Guss, R. F. Mahrt, H. Bässler, M. Porsch, J. Daub, *Adv. Mater.* **1995**, *7*, 551.

[79] C. M. Cardona, W. Li, A. E. Kaifer, D. Stockdale, G. C. Bazan, *Adv. Mater.* **2011**, *23*, 2367.

Supporting Information

Preparation of Near-Infrared Emissive π-Conjugated Polymer Films Based on Boron-Fused Azobenzene Complexes with Perpendicularly Protruded Aryl Substituents

Masayuki Gon, Junko Wakabayashi, Masashi Nakamura, Kazuo Tanaka* and Yoshiki Chujo

Department of Polymer Chemistry, Graduate School of Engineering, Kyoto University Katsura, Nishikyo-ku, Kyoto 615-8510, Japan

E-mail: tanaka@poly.synchem.kyoto-u.ac.jp

Contents page

General S–3

Materials S–4

Synthetic procedures and characterization S–5

BAz-C6F5 S–5

P-BAz-C6F5 S–8

BAz-Ph S–11

P-BAz-Ph S–14

BAz-Mes S–17

P-BAz-Mes S–20

UV–vis absorption spectra of **BAz** polymers S–23

PL absorption spectra of **BAz** complexes S–23

PL lifetime decay curves S–24

Computational details for theoretical calculation S–25

Results of representative transitions of **BAz** complexes S–26

Molecular orbitals of **BAz** complexes S–27

Selected Kohn–Sham orbitals of model compounds S–28

References S–29

General

^{1}H, ^{13}C and ^{11}B NMR spectra were recorded on JEOL EX400 and AL400 instruments at 400, 100 and 128 MHz, respectively. Samples were analyzed in $CDCl_3$. The chemical shift values were expressed relative to Me_4Si for ^{1}H and ^{13}C NMR as an internal standard in $CDCl_3$ and $BF_3{\cdot}Et_2O$ for ^{11}B NMR as a capillary standard. Analytical thin layer chromatography (TLC) was performed with silica gel 60 Merck F254 plates. Column chromatography was performed with Wakogel® C-300 silica gel. High-resolution mass (HRMS) spectrometry was performed at the Technical Support Office (Department of Synthetic Chemistry and Biological Chemistry, Graduate School of Engineering, Kyoto University), and the HRMS spectra were obtained on a Thermo Fisher Scientific EXACTIVE spectrometer for electrospray ionization (ESI) and a Thermo Fisher Scientific EXACTIVE spectrometer for atmospheric pressure chemical ionization (APCI). UV–vis spectra were recorded on a SHIMADZU UV-3600 spectrophotometer, and samples were analyzed at room temperature. Fluorescence emission spectra were recorded on a HORIBA Scientific Fluorolog-3 spectrofluorometer and samples were analyzed at room temperature. Absolute photoluminescence quantum efficiency (Φ_{PL}) was recorded on a Hamamatsu Photonics Quantaurus-QY Plus C13534-01. The PL lifetime measurement was performed on a Horiba FluoreCube spectrofluorometer system; excitation was carried out using UV and visible diode lasers (NanoLED 375 nm and 532 nm). Cyclic voltammetry (CV) was carried out on a BASALS-Electrochemical-Analyzer Model 600D with a grassy carbon working electrode, a Pt counter electrode, an Ag/AgCl reference electrode, and the ferrocene/ferrocenium (Fc/Fc^{+}) external reference at a scan rate of 0.1 V s^{-1}. The NIR filter (SCF-50S-70R) was purchased from SIGMAKOKI CO.,LTD.

Materials

Commercially available compounds used without purification:

4-Bromo-2-methoxy aniline (**1**) (FUJIFILM Wako Pure Chemical Industries, Ltd.)

Manganese(IV) Oxide, Powder (MnO_2) (FUJIFILM Wako Pure Chemical Industries, Ltd.)

Boron tribromide (17% in CH_2Cl_2, ca. 1 M) (BBr_3 in CH_2Cl_2) (Tokyo Chemical Industry Co, Ltd.)

Dimesitylfluoroborane (FUJIFILM Wako Pure Chemical Industries, Ltd.)

Dichlorophenylborane (FUJIFILM Wako Pure Chemical Industries, Ltd.)

2,3,4,5,6-Pentafluorophenylboronic acid (FUJIFILM Wako Pure Chemical Industries, Ltd.)

$Pd_2(dba)_3$ (dba = dibenzylideneacetone) (Tokyo Chemical Industry Co, Ltd.)

2-Dicyclohexylphosphino-2′,4′,6′-triisopropylbiphenyl (XPhos) (Strem Chemicals, Inc.)

Commercially available solvents:

MeOH (FUJIFILM Wako Pure Chemical Industries, Ltd.), toluene (deoxidized grade, FUJIFILM Wako Pure Chemical Industries, Ltd.) CH_2Cl_2 (deoxidized grade, FUJIFILM Wako Pure Chemical Industries, Ltd.) used without purification. Et_3N (Kanto Chemical Co., Inc.), purified by passage through solvent purification columns under N_2 pressure.

Compounds prepared as described in the literatures:

6,6′-(Diazene-1,2-diyl)bis(3-bromophenol) (**L-Az**) [1]

5,5′-Bis(trimethylstannyl)-3,3′-didodecyl-2,2′-bithiophene (**BT**) [2],[3]

Synthetic Procedures and Characterization

Synthesis of BAz-C6F5

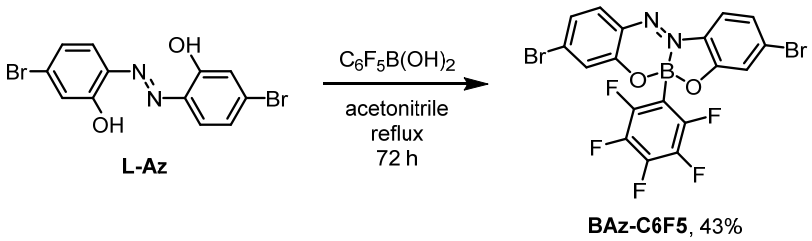

BAz-C6F5, 43%

6,6′-(Diazene-1,2-diyl)bis(3-bromophenol) (**L-Az**) (186 mg, 0.50 mmol) and 2,3,4,5,6-pentafluorophenylboronic acid (212 mg, 1.00 mmol) were placed in a round-bottom flask equipped with a magnetic stirring bar. After degassing and filling N_2 three times, acetonitrile (25 mL) was added to the flask and refluxed for 72 h. After the reaction, the solvent was removed with a rotary evaporator. The residue was semi-purified by column chromatography on SiO_2 (CH_2Cl_2/hexane = 1/2 v/v) and further purification was carried out by recrystallization with hexane to afford **BAz-C6F5** (117 mg, 0.21 mmol, 43%) as a red crystal.

R_f = 0.63 (CH_2Cl_2/hexane = 1/2 v/v). ^{1}H NMR ($CHCl_3$, 400 MHz) δ 7.72 (d, J = 8.8 Hz, 1H), 7.71 (d, J = 8.5 Hz, 1H), 7.39 (d, J = 2.0 Hz, 1H), 7.37 (d, J = 1.6 Hz, 1H), 7.30 (dd, J = 8.8, 1.9 Hz, 1H), 7.25 (dd, J = 8.6, 1.7 Hz, 1H) ppm; ^{13}C NMR ($CDCl_3$, 100 MHz) δ 162.1, 148.2 (d, $J_{C\text{-}F}$ = 244.3 Hz), 144.3, 141.0 (d, $J_{C\text{-}F}$ = 251.7 Hz), 139.6, 137.1 (d, $J_{C\text{-}F}$ = 249.2 Hz), 133.4, 132.6, 132.3, 131.8, 126.7, 125.8, 123.7, 120.0, 117.9 ppm; ^{11}B NMR ($CDCl_3$, 128 MHz) δ 4.02 ppm. HRMS (ESI) calcd. for $C_{18}H_6BBr_2F_5N_2O_2$ $[M]^-$: 545.8815, found: 545.8815.

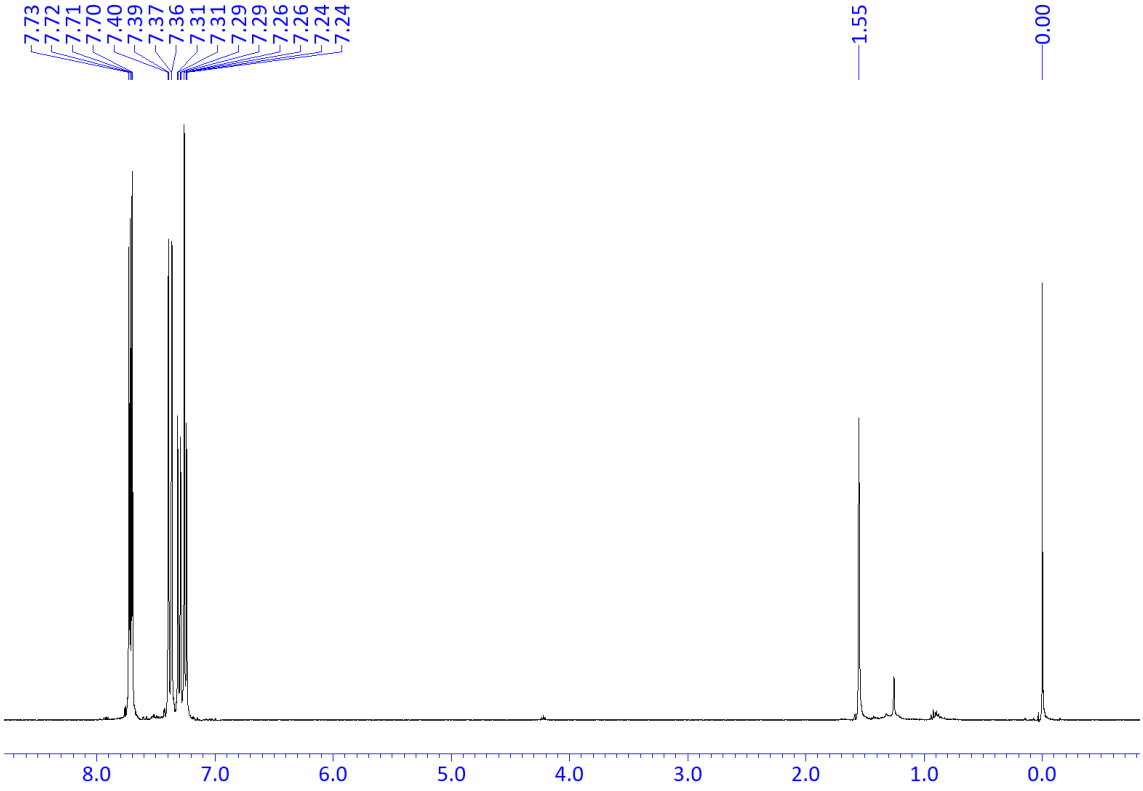

Chart 1. ^{1}H NMR spectrum of **BAz-C6F5** in $CDCl_3$.

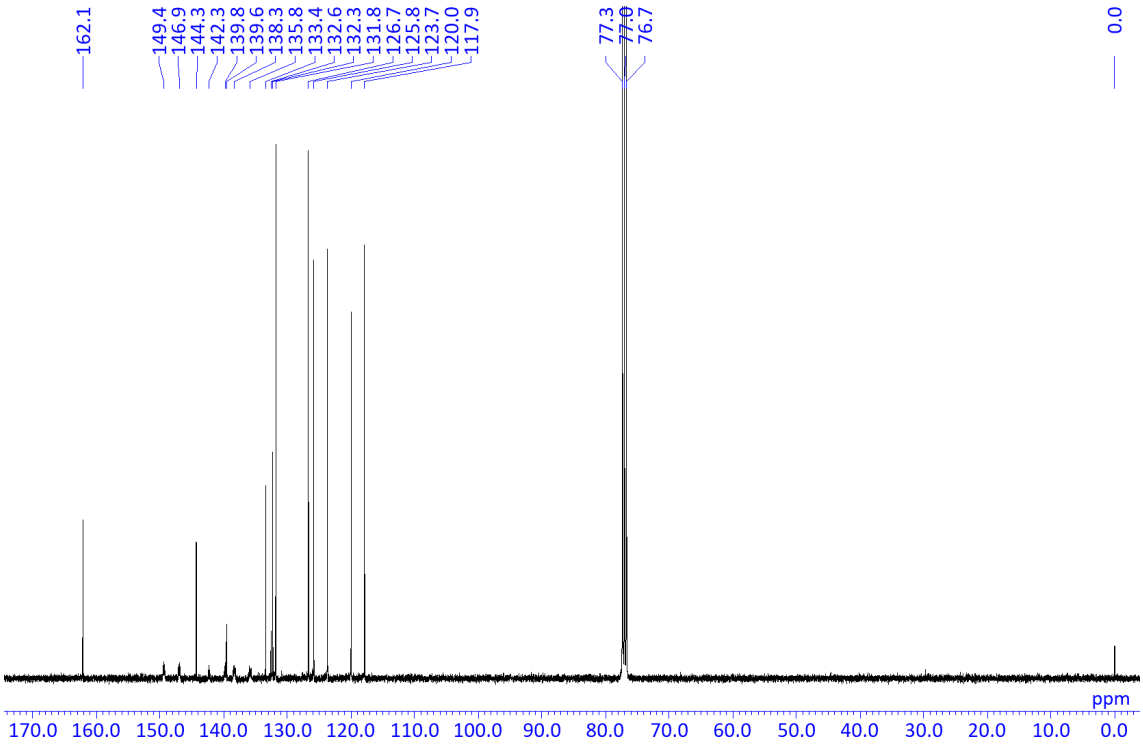

Chart 2. ^{13}C NMR spectrum of **BAz-C6F5** in $CDCl_3$.

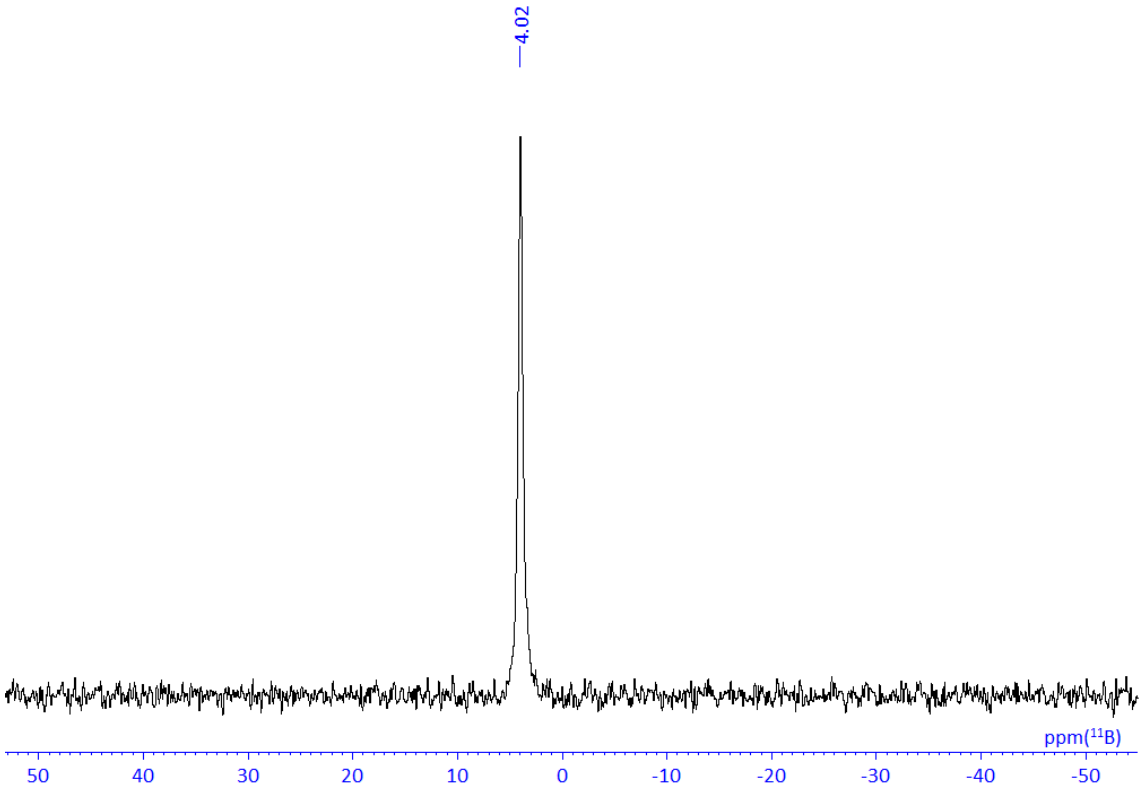

Chart 3. ^{11}B NMR spectrum of **BAz-C6F5** in $CDCl_3$.

Synthesis of P-BAz-C6F5

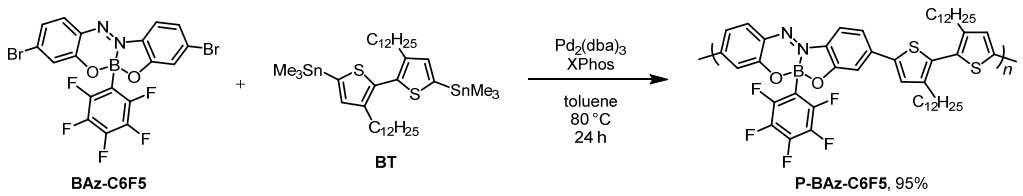

A mixture of **BAz-C6F5** (27.4 mg, 0.050 mmol), 5,5′-bis(trimethylstannyl)-3,3′-didodecyl-2,2′-bithiophene (**BT**) (41.4 mg, 0.050 mmol), $Pd_2(dba)_3$ (1.4 mg, 0.0015 mmol), XPhos (1.4 mg, 0.0030 mmol) was placed in a round-bottom flask equipped with a magnetic stirring bar. After degassing and filling Ar three times, toluene (1.0 mL) was added to the mixture. The reaction was carried out at 80 °C for 24 h. After the reaction, the obtained polymer was redissolved in a small amount of $CHCl_3$, and then the product was reprecipitated from MeOH. The polymer collected by filtration was dried *in vacuo* to afford **P-BAz-C6F5** (42.2 mg, 95%) as a black solid.

M_n = 15,900, M_w = 39,100, M_w/M_n = 2.5. ^{1}H NMR ($CDCl_3$, 400 MHz) δ 7.85 (d, J = 8.8 Hz, 1H), 7.81 (d, J = 8.8 Hz, 1H), 7.44–7.38 (br, 6H), 2.60 (br, 4H), 1.61 (br, 4H), 1.29–1.23 (br, 36H), 0.86 (t, J = 6.8 Hz, 6H) ppm; ^{13}C NMR ($CDCl_3$, 100 MHz) δ 162.0, 149.4, 147.0, 145.0, 144.8, 144.8, 144.6, 114.6, 143.0, 142.7, 142.6, 142.3, 142.2, 142.0, 140.3, 139.5, 138.2, 135.9, 132.9, 131.9, 131.8, 131.5, 131.1, 130.9, 128.4, 127.7, 120.1, 120.0, 117.4, 115.6, 111.6, 31.9, 30.7, 29.7, 29.7, 29.6, 29.4, 29.4, 29.2, 22.7, 14.1 ppm; ^{11}B NMR ($CDCl_3$, 128 MHz) δ 3.83 ppm.

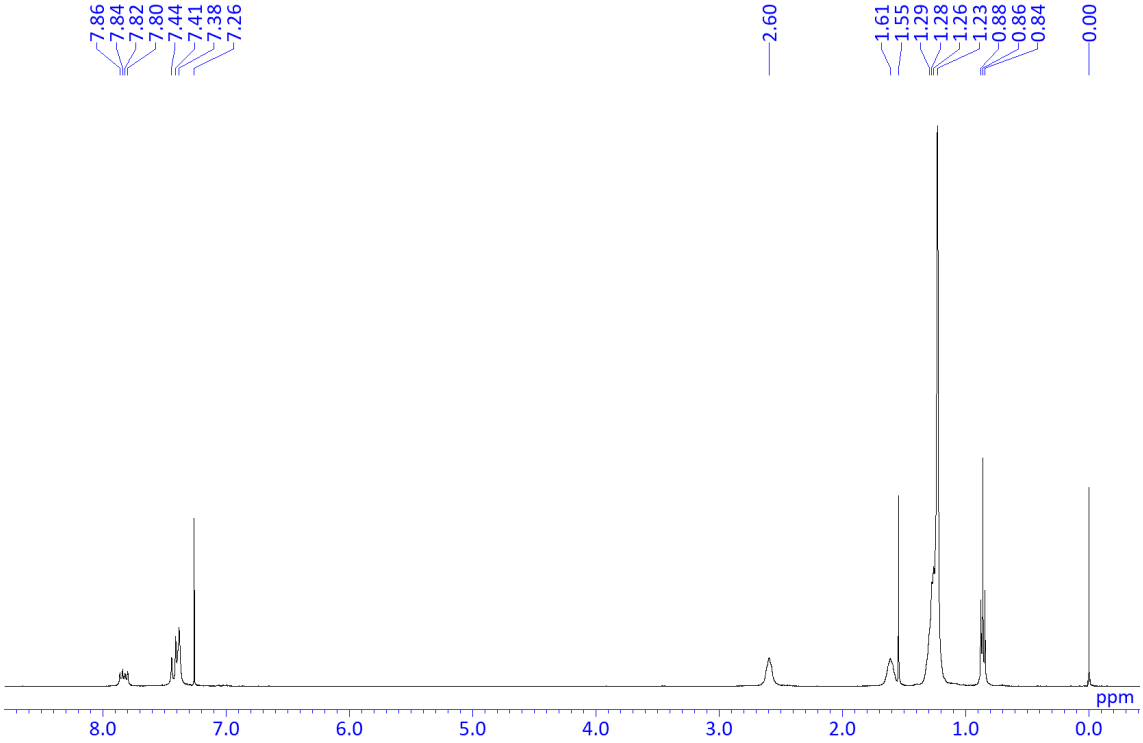

Chart 4. ^{1}H NMR spectrum of **P-BAz-C6F5** in $CDCl_3$.

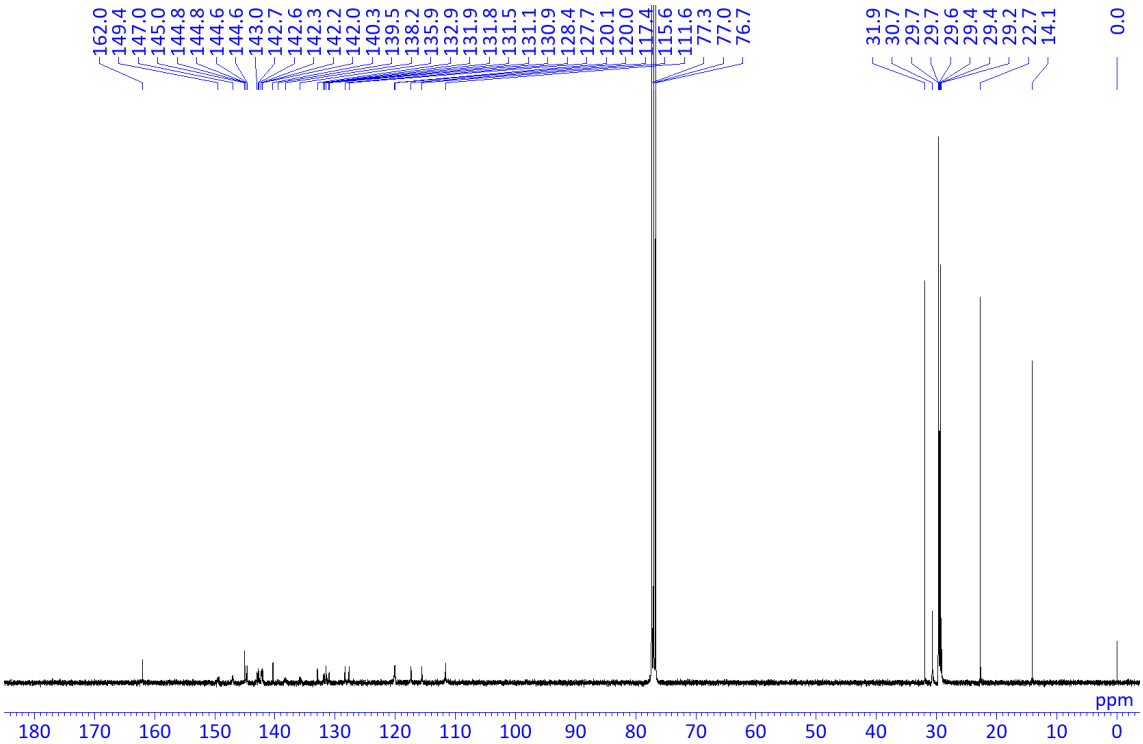

Chart 5. ^{13}C NMR spectrum of **P-BAz-C6F5** in $CDCl_3$.

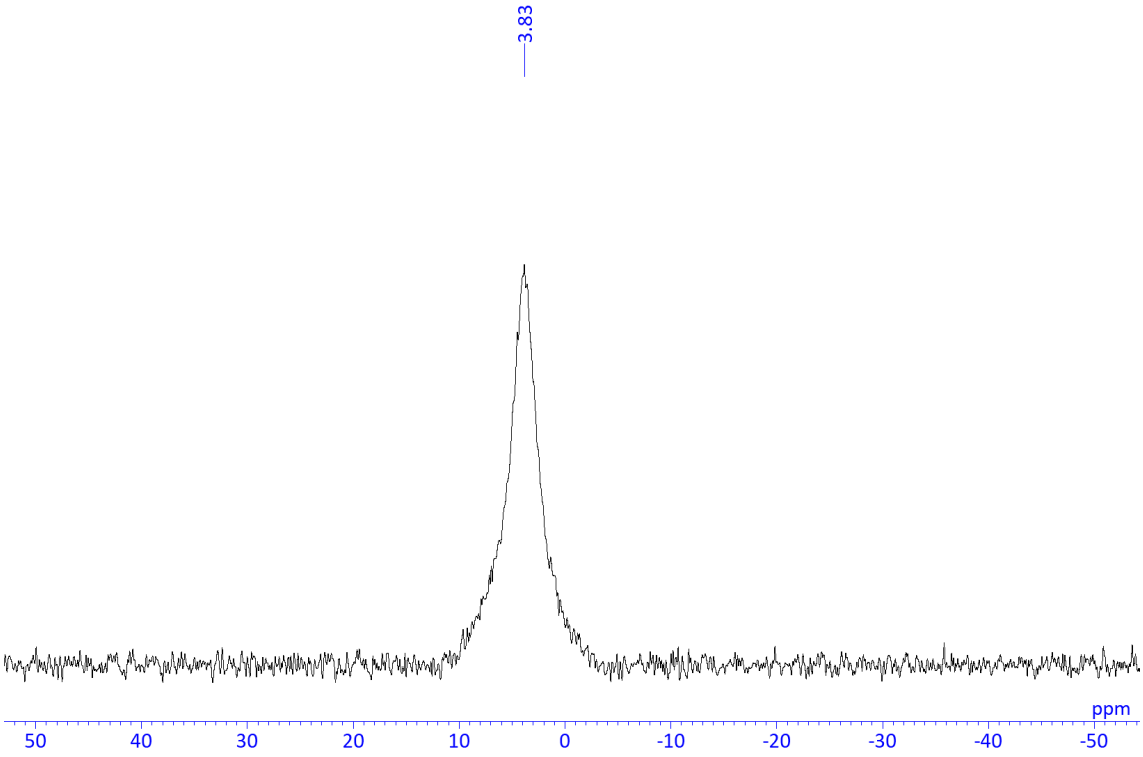

Chart 6. ^{11}B NMR spectrum of **P-BAz-C6F5** in $CDCl_3$.

Synthesis of BAz-Ph

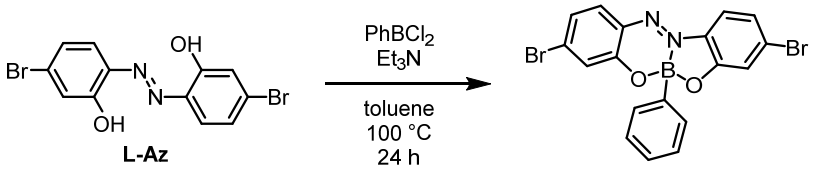

6,6′-(Diazene-1,2-diyl)bis(3-bromophenol) (**L-Az**) (372 mg, 1.00 mmol) was placed in a round-bottom flask equipped with a magnetic stirring bar. After degassing and filling N_2 three times, toluene (90 mL) was added to the flask. Dichlorophenylborane (0.40 mL, 3.00 mmol) and Et_3N (0.21 mL, 1.5 mmol) were added to the mixture. After finishing the addition, the reaction was carried out at 100 °C for 17 h. After the reaction, MeOH was added for quenching the reaction, and the solvent was removed with a rotary evaporator. The residue was semi-purified by column chromatography on SiO_2 (CH_2Cl_2/hexane = 1/2 v/v as an eluent) and further purification was carried out by recrystallization with hexane to afford **BAz-Ph** (377 mg, 0.823 mmol, 82%) as a dark red crystal.

R_f = 0.38 (CH_2Cl_2/hexane = 1/2 v/v). ^{1}H NMR ($CHCl_3$, 400 MHz) δ 7.65 (d, J = 8.6 Hz, 1H), 7.59 (d, J = 8.8 Hz, 1H), 7.42 (d, J = 2.0Hz, 1H), 7.40 (d, J = 1.7 Hz, 1H), 7.24–7.14 (m, 7H) ppm; ^{13}C NMR ($CDCl_3$, 100 MHz) δ 163.0, 146.3, 139.4, 132.7, 132.5, 132.1, 131.9, 131.6, 128.7, 127.8, 125.6, 125.1, 123.4, 119.9, 117.8 ppm; ^{11}B NMR ($CDCl_3$, 128 MHz) δ 6.38 ppm. HRMS (ESI) calcd. for $C_{18}H_{11}BBr_2N_2NaO_2$ $[M+Na]^+$: 478.9178, found: 478.9167.

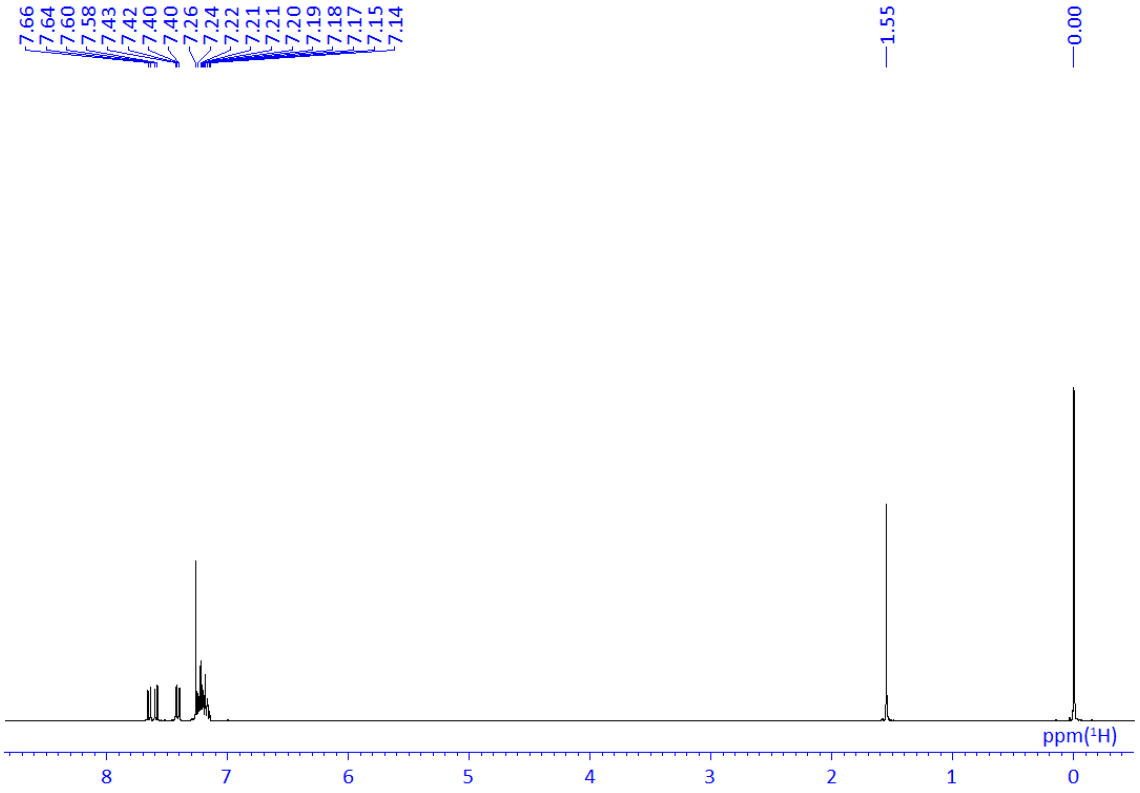

Chart 7. ^{1}H NMR spectrum of **BAz-Ph** in $CDCl_3$.

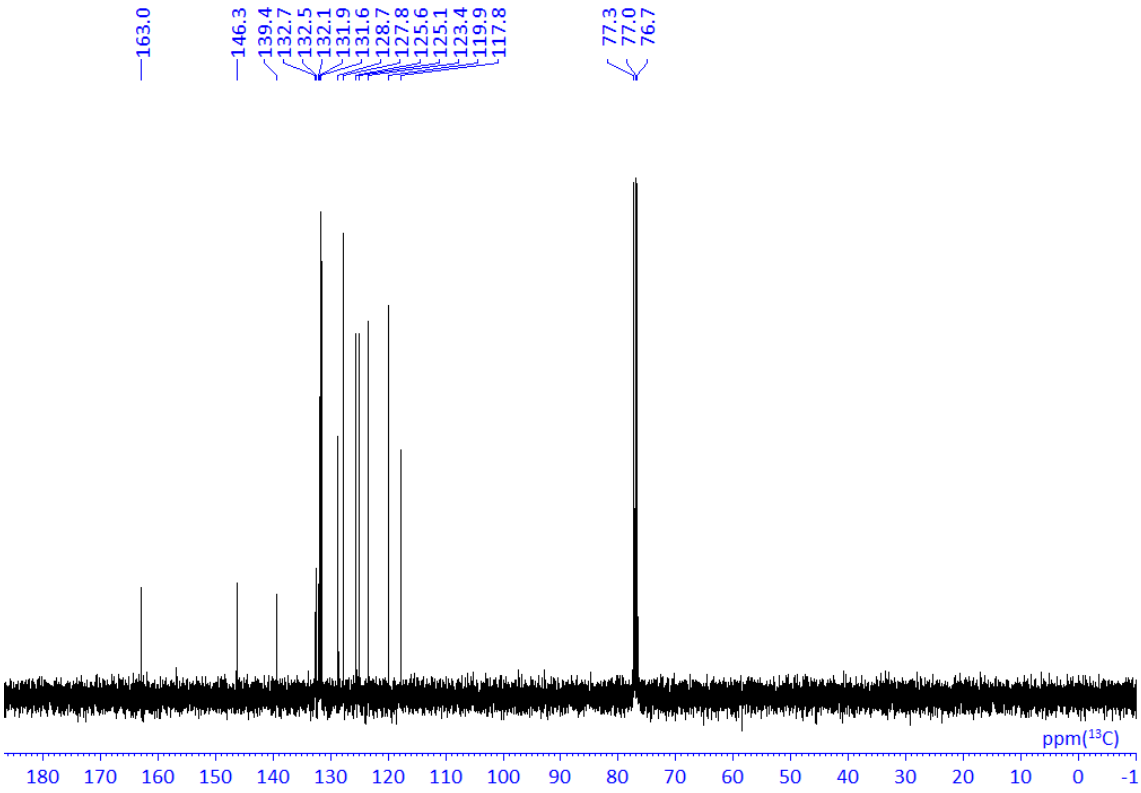

Chart 8. ^{13}C NMR spectrum of **BAz-Ph** in $CDCl_3$.

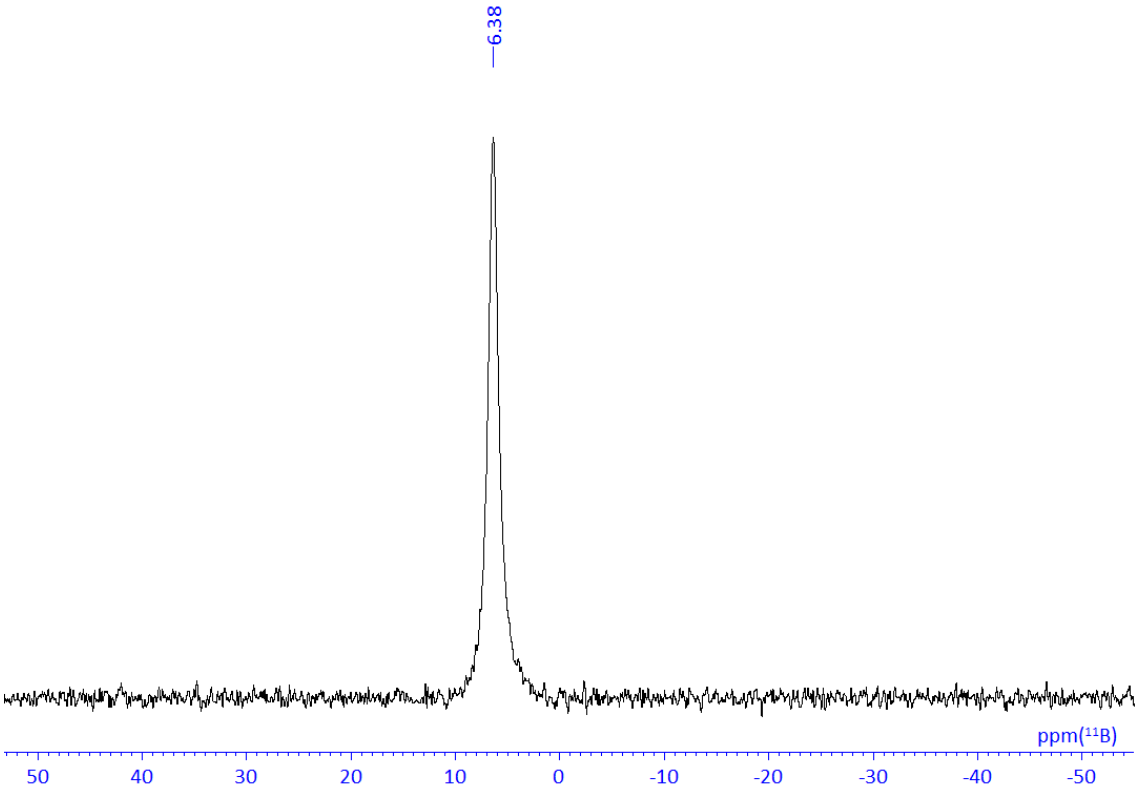

Chart 9. ^{11}B NMR spectrum of **BAz-Ph** in $CDCl_3$.

Synthesis of P-BAz-Ph

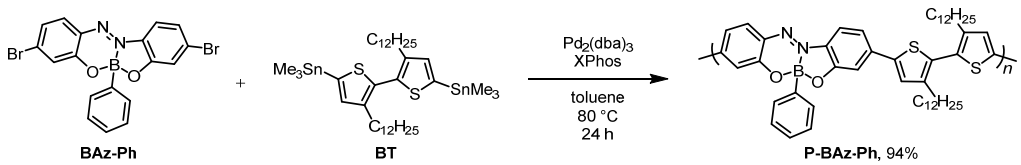

A mixture of **BAz-Ph** (45.8 mg, 0.10 mmol), 5,5′-bis(trimethylstannyl)-3,3′-didodecyl-2,2′-bithiophene (**BT**) (82.9 mg, 0.10 mmol), $Pd_2(dba)_3$ (2.7 mg, 0.0030 mmol), XPhos (2.9 mg, 0.0060 mmol) was placed in a round-bottom flask equipped with a magnetic stirring bar. After degassing and filling N_2 three times, toluene (2.0 mL) was added to the mixture. The reaction was carried out at 80 °C for 24 h. After the reaction, the obtained polymer was redissolved in a small amount of $CHCl_3$, and then the product was reprecipitated from MeOH. The polymer collected by filtration was dried *in vacuo* to afford **P-BAz-Ph** (74.8 mg, 94%) as a black solid.

M_n = 13,800, M_w = 29,800, M_w/M_n = 2.2. ^{1}H NMR ($CDCl_3$, 400 MHz) δ 7.78 (d, J = 8.3 Hz, 1H), 7.70 (d, J = 8.5 Hz, 1H), 7.47–7.32 (br, 7H), 7.21–7.15 (br, 4H), 2.61 (br, 4H), 1.63 (br, 4H), 1.24 (br, 36H), 0.86 (t, J = 6.6 Hz, 6H) ppm; ^{13}C NMR ($CDCl_3$, 100 MHz) δ 162.9, 146.9,144.6, 144.5, 142.8, 142.4, 142.2, 140.3, 133.2, 131.8, 131.6, 131.4, 131.3, 130.8, 128.3, 127.9, 127.7, 127.4, 119.4, 119.1, 117.3, 115.5, 111.7, 31.9, 30.7, 29.7, 29.7, 29.6, 29.5, 29.4, 29.4, 29.2, 22.7, 14.1 ppm; ^{11}B NMR ($CDCl_3$, 128 MHz) δ 5.30 ppm.

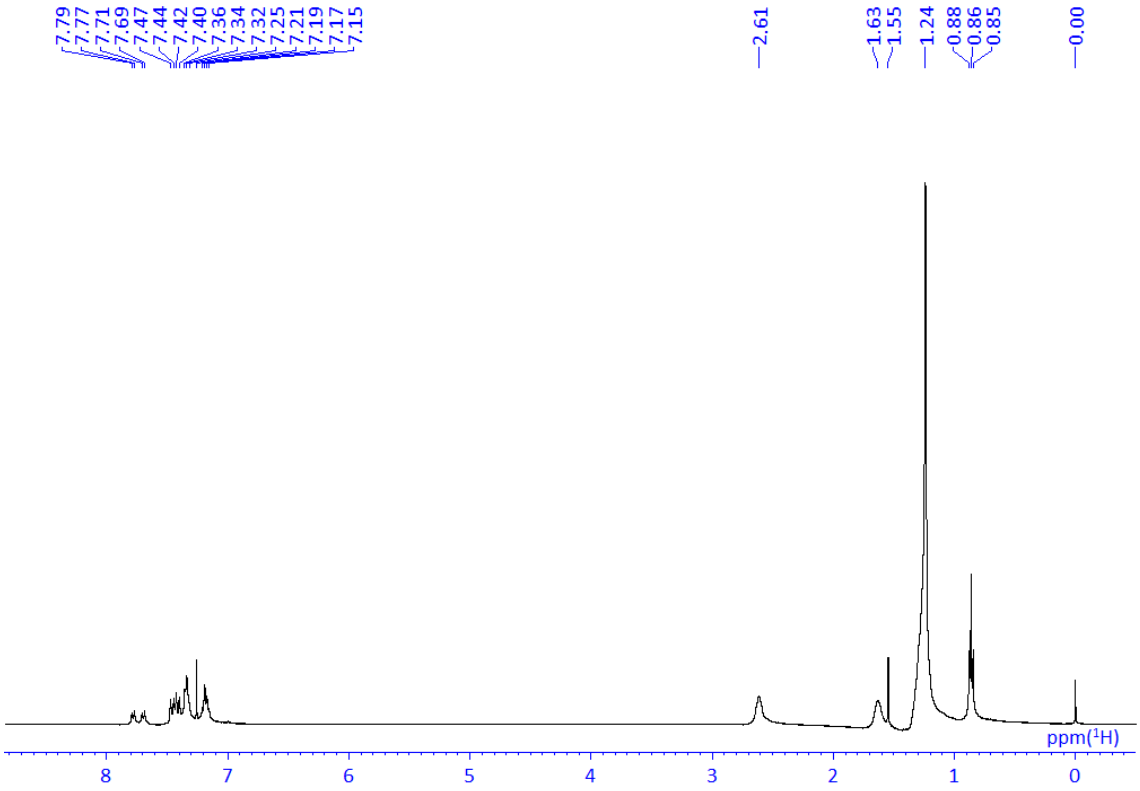

Chart 10. ^{1}H NMR spectrum of **P-BAz-Ph** in $CDCl_3$.

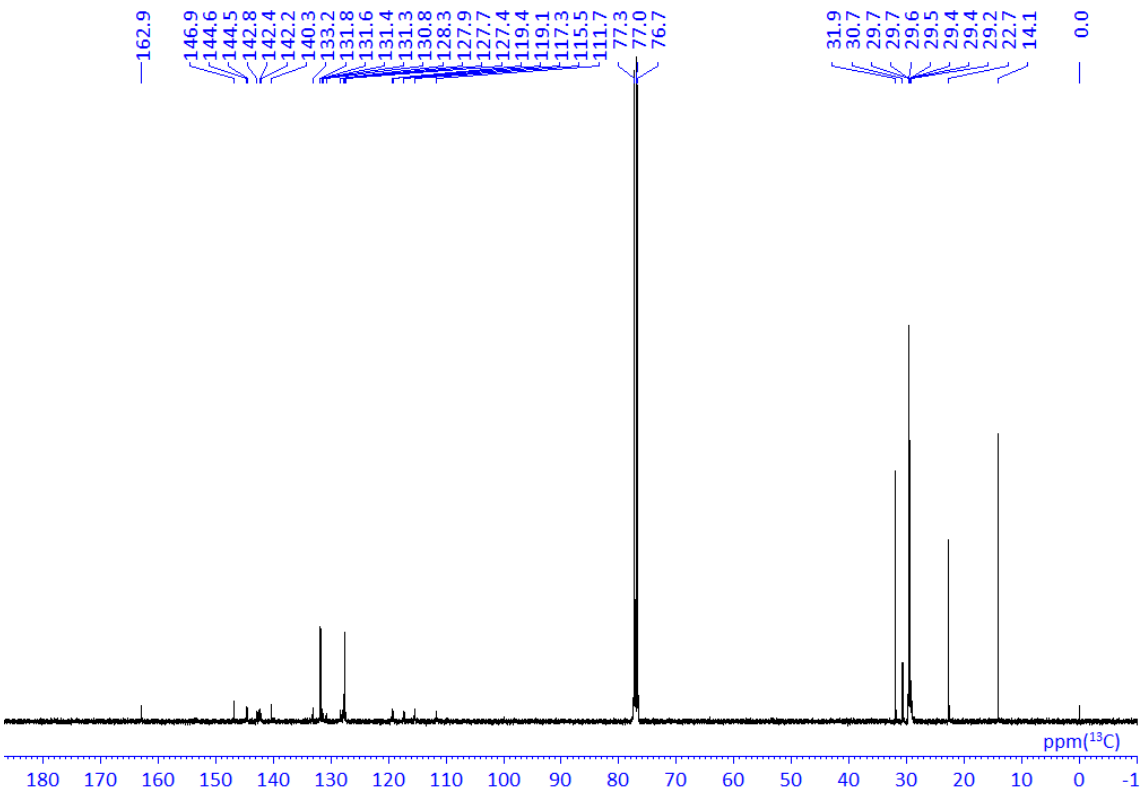

Chart 11. ^{13}C NMR spectrum of **P-BAz-Ph** in $CDCl_3$.

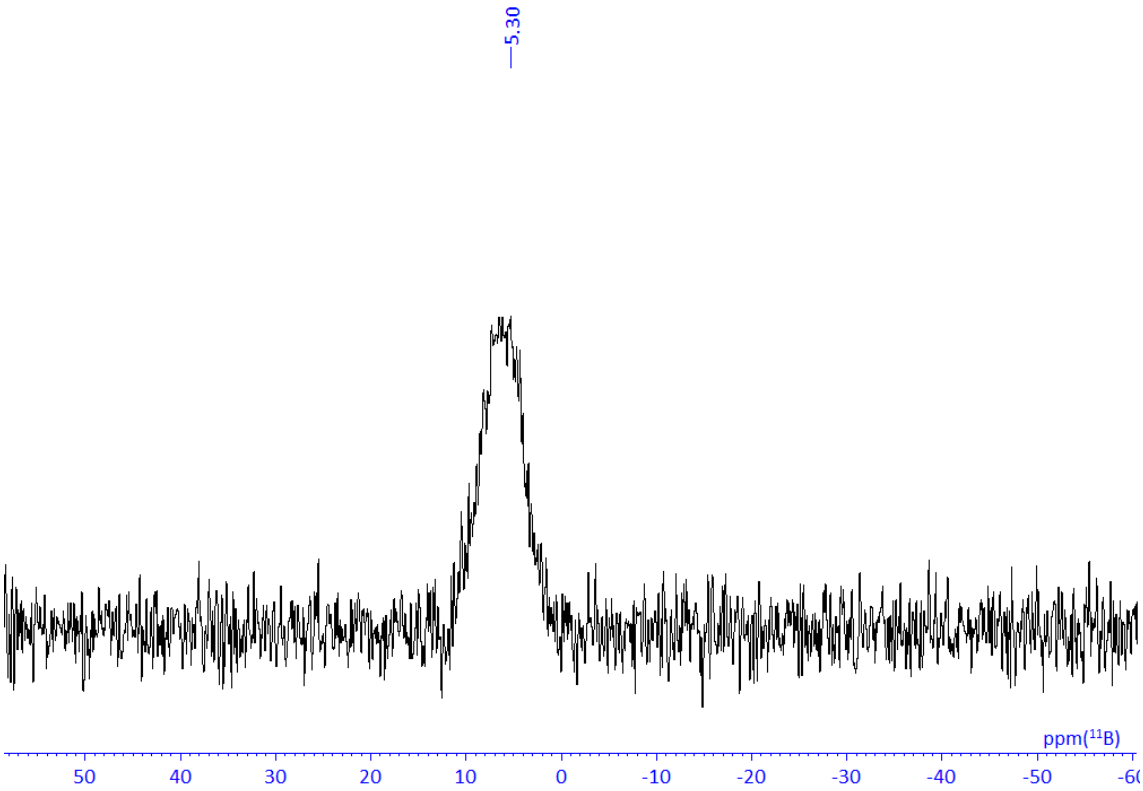

Chart 12. ^{11}B NMR spectrum of **P-BAz-Ph** in $CDCl_3$.

Synthesis of BAz-Mes

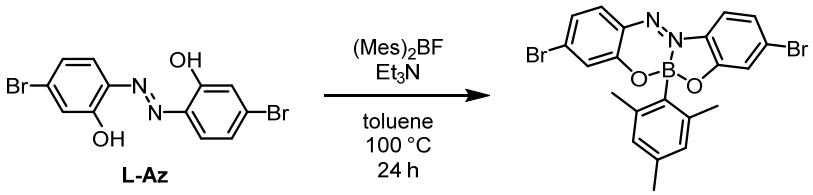

L-Az (50 mg, 0.20 mmol) and dimesitylfluoroborane were placed in a round-bottom flask equipped with a magnetic stirring bar. After degassing and filling Ar three times, toluene (50 mL) was added to the flask, then Et_3N (0.10 mL, 0.75 mmol) was added to the mixture. After finishing the addition, the reaction was carried out at 100 °C for 24 h. After the reaction, the solvent was removed with a rotary evaporator. The residue was purified by column chromatography on SiO_2 (CH_2Cl_2/hexane = 1/1 v/v) to afford **BAz-Mes** (110 mg, 0.22 mmol, 44%) as a dark red solid.

R_f = 0.39 (CH_2Cl_2/hexane = 1/2 v/v). ^{1}H NMR ($CHCl_3$, 400 MHz) δ 7.67 (d, J = 8.6 Hz, 1H), 7.63 (d, J = 8.8 Hz, 1H), 7.27 (d, J = 1.7 Hz, 1H), 7.25 (d, J = 1.9 Hz, 1H), 7.17 (dd, J = 9.0, 2.0 Hz, 1H), 7.15 (dd, J = 8.8, 1.7 Hz, 1H), 6.65 (s, 2H), 2.35 (s, 6H), 2.14 (s, 3H) ppm; ^{13}C NMR ($CDCl_3$, 100 MHz) δ 162.7, 150.0, 141.1, 140.2, 137.1, 133.2, 132.7, 131.5, 131.1, 129.2, 125.8, 124.8, 123.5, 120.3, 117.8, 22.9, 20.8 ppm; NMR ($CDCl_3$, 128 MHz) δ 6.67 ppm. HRMS (ESI) calcd. for $C_{21}H_{17}BBr_2N_2O_2$ $[M]^-$: 497.9750, found: 497.9758.

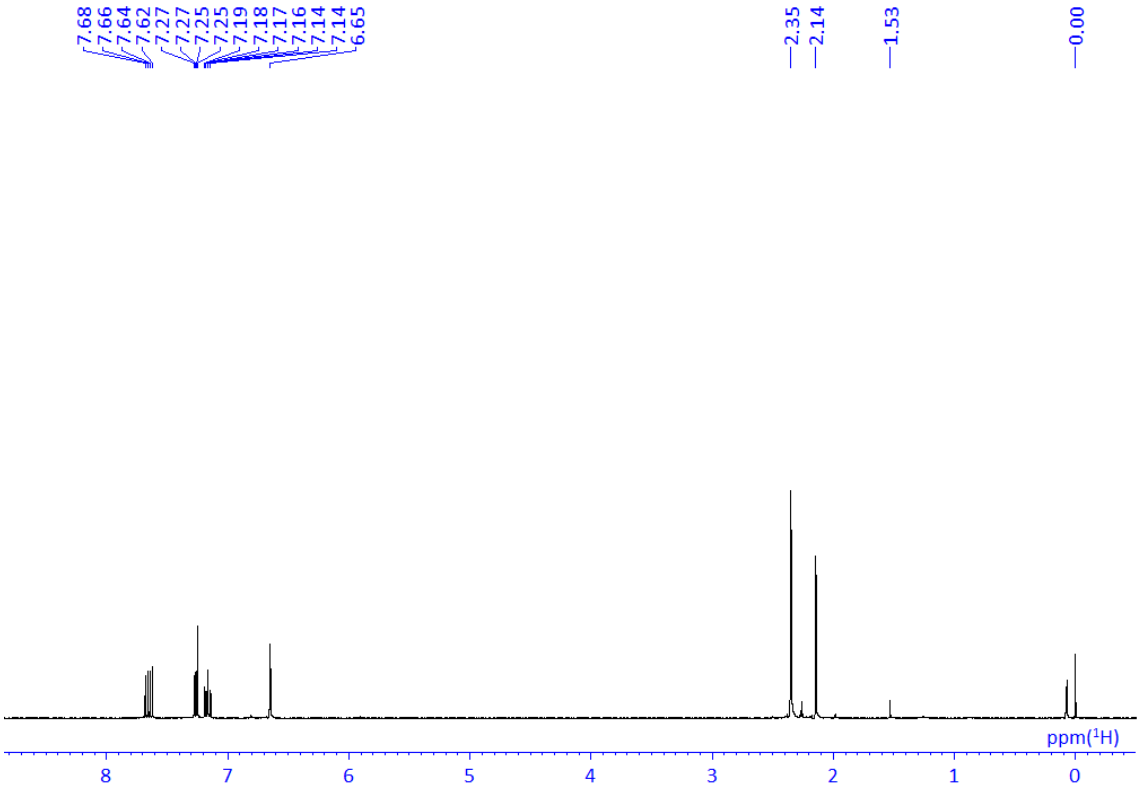

Chart 13. ^{1}H NMR spectrum of **BAz-Mes** in $CDCl_3$.

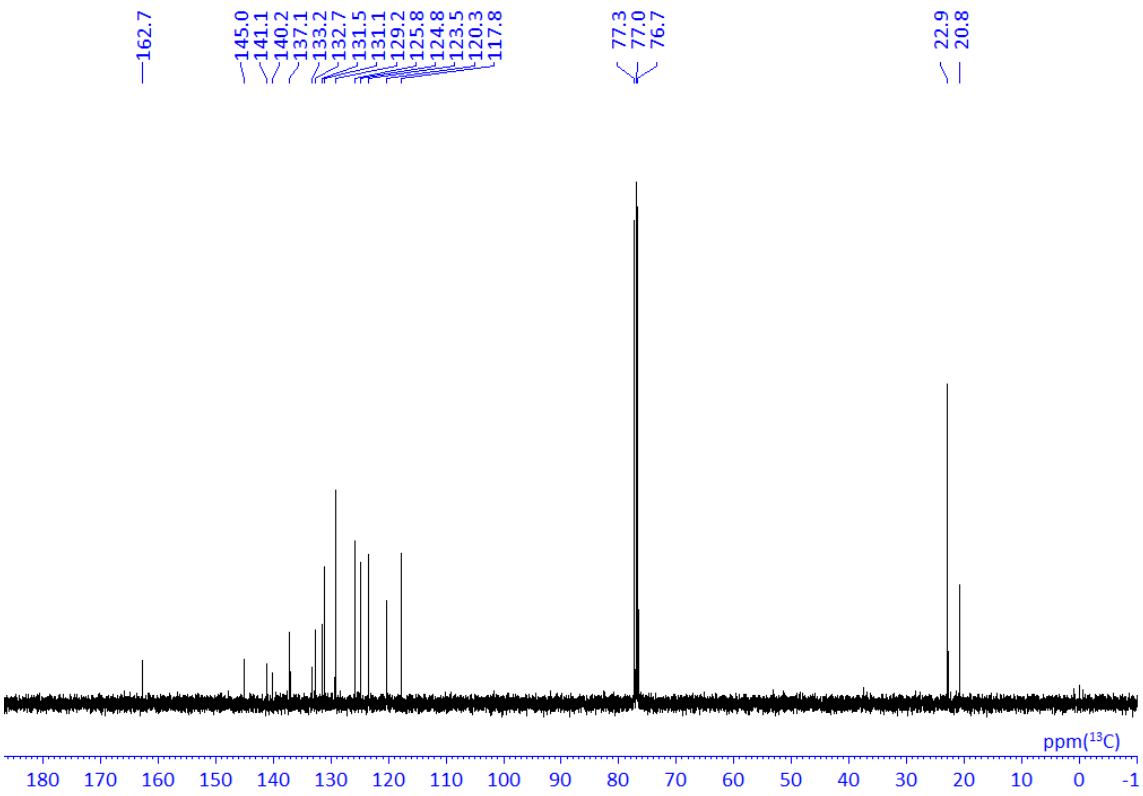

Chart 14. ^{13}C NMR spectrum of **BAz-Mes** in $CDCl_3$.

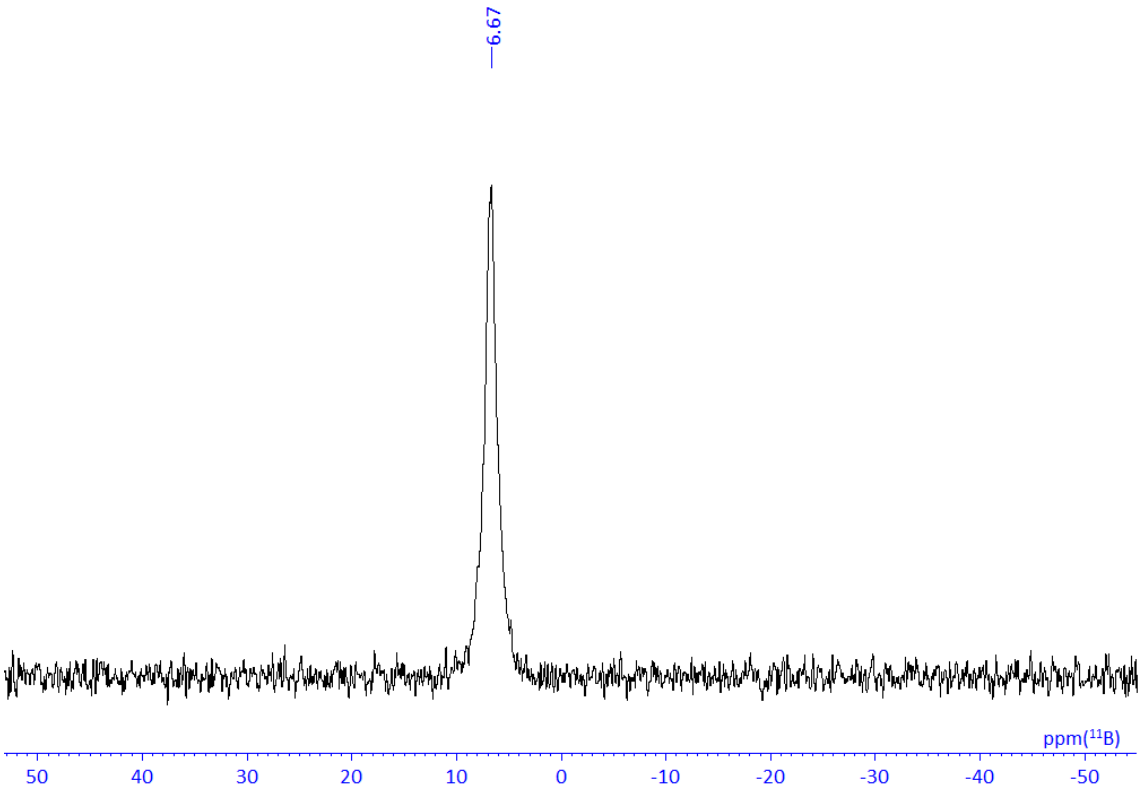

Chart 15. ^{11}B NMR spectrum of **BAz-Mes** in $CDCl_3$.

Synthesis of P-BAz-Mes

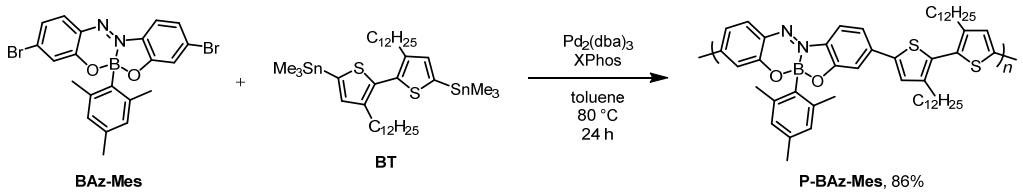

A mixture of **BAz-Mes** (50.0 mg, 0.10 mmol), 5,5′-bis(trimethylstannyl)-3,3′-didodecyl-2,2′-bithiophene (**BT**) (82.9 mg, 0.10 mmol), $Pd_2(dba)_3$ (2.7 mg, 0.0030 mmol), XPhos (2.9 mg, 0.0060 mmol) was placed in a round-bottom flask equipped with a magnetic stirring bar. After degassing and filling Ar three times, toluene (2.0 mL) was added to the mixture. The reaction was carried out at 80 °C for 24 h. After the reaction, the obtained polymer was redissolved in a small amount of $CHCl_3$, and then the product was reprecipitated from MeOH. The polymer collected by filtration was dried *in vacuo* to afford **P-BAz-Mes** (72.0 mg, 86%) as a black solid.

M_n = 17,200, M_w = 45,100, M_w/M_n = 2.6. ^{1}H NMR ($CDCl_3$, 400 MHz) δ 7.80 (d, J = 9.3 Hz, 1H), 7.74 (d, J = 8.8 Hz, 1H), 7.33–7.24 (br, 6H), 6.66 (s, 2H), 2.56 (br, 4H), 2.44 (s, 6H), 2.14 (s, 3H), 1.58 (br, 4H), 1.23 (br, 36H), 0.86 (t, J = 5.8 Hz, 6H) ppm; ^{13}C NMR ($CDCl_3$, 100 MHz) δ 162.6, 145.6, 144.4, 142.9, 142.5, 142.3, 141.7, 141.3, 141.1, 140.0, 136.7, 133.7, 130.7, 129.2, 127.8, 127.2, 119.5, 119.2, 117.2, 115.5, 112.1, 31.9, 30.7, 29.7, 29.7, 29.7, 29.6, 29.4, 29.4, 29.4, 29.2, 23.0, 22.7, 20.8, 14.1 ppm; ^{11}B NMR ($CDCl_3$, 128 MHz) δ 3.44 ppm.

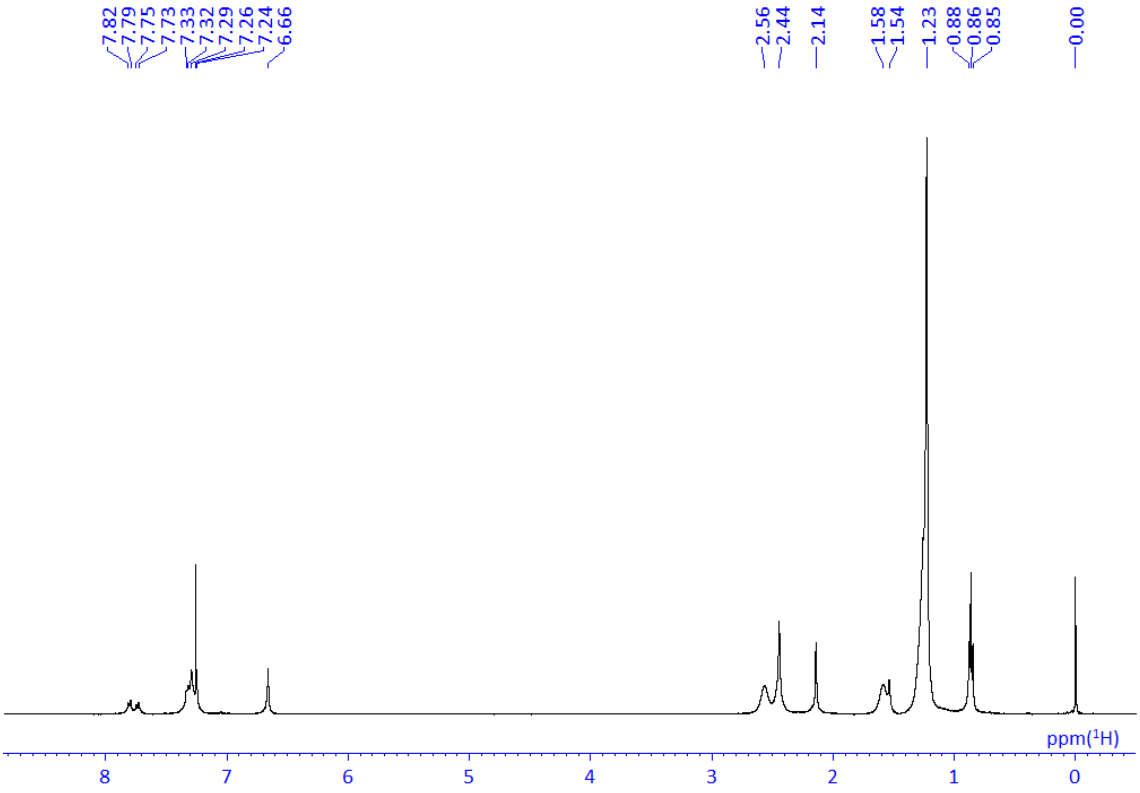

Chart 16. ^{1}H NMR spectrum of **P-BAz-Mes** in $CDCl_3$.

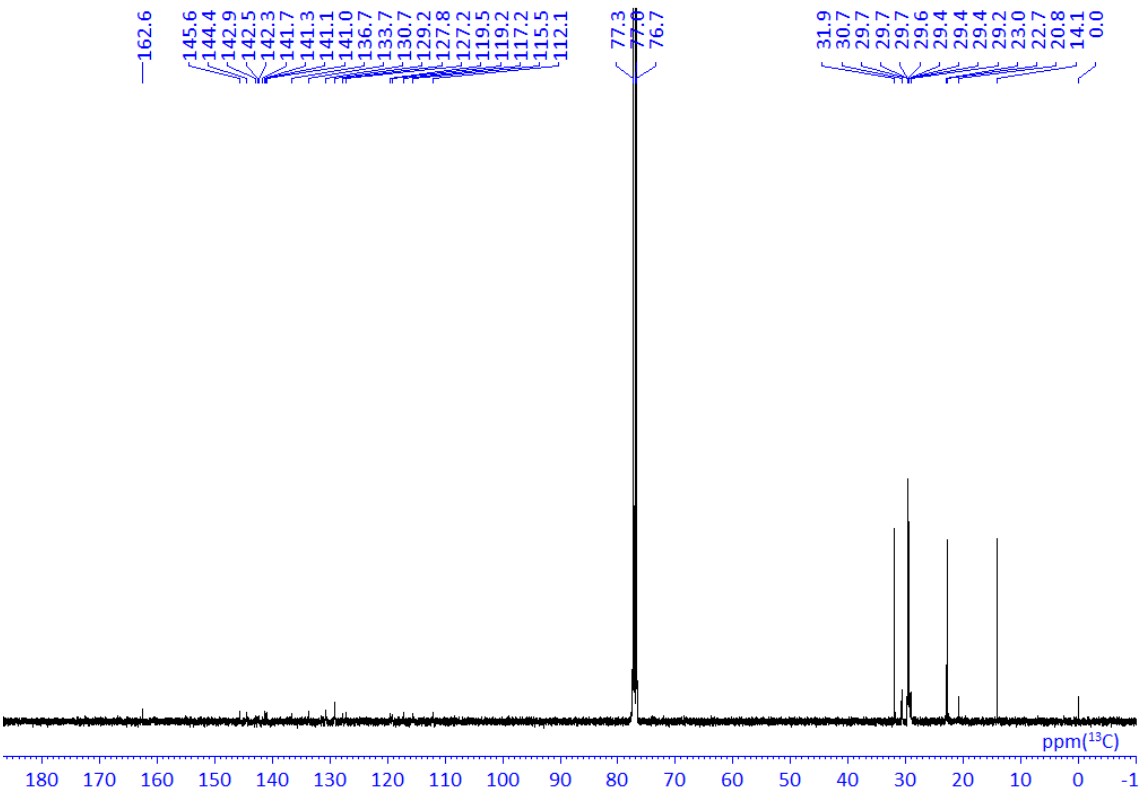

Chart 17. ^{13}C NMR spectrum of **P-BAz-Mes** in $CDCl_3$.

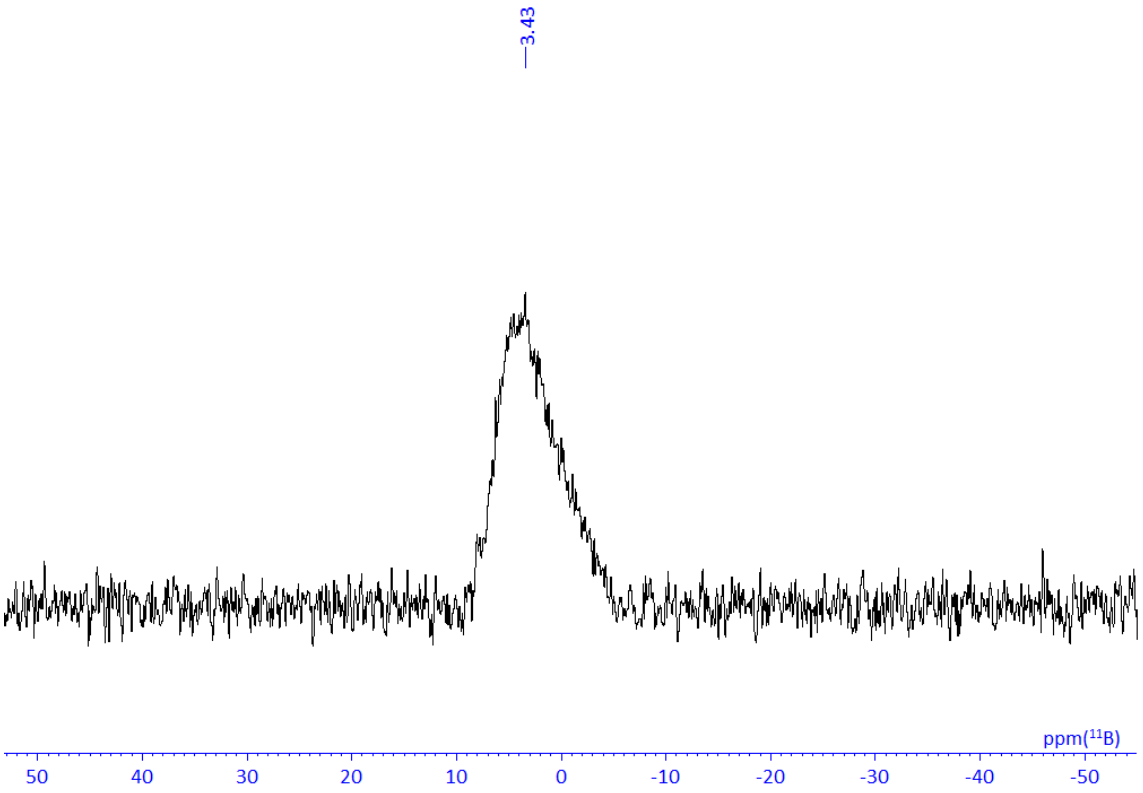

Chart 18. ^{11}B NMR spectrum of **P-BAz-Mes** in $CDCl_3$.

UV–vis absorption spectra of BAz polymers

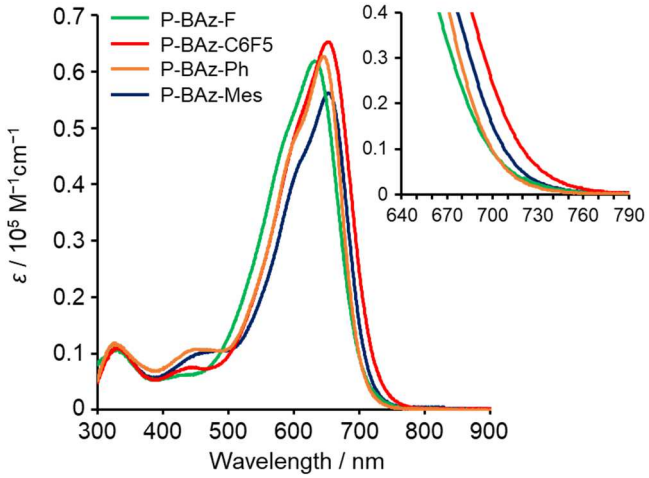

Figure S1. UV–vis absorption spectra of **BAz** polymers in toluene (1.0×10^{-5} M per repeating unit). The inserted chart denotes enlarged view at edge of the spectra for estimation of optical band gaps.

PL spectra of BAz complexes

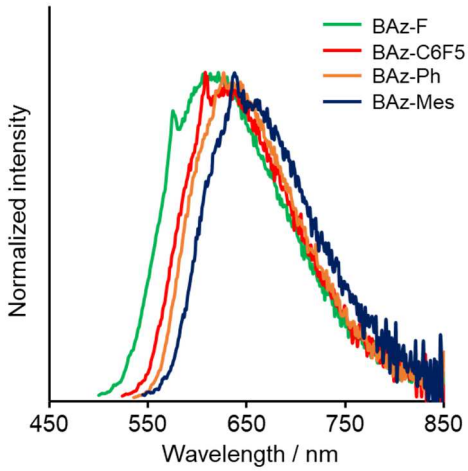

Figure S2. PL spectra of **BAz** complexes in toluene (1.0×10^{-5} M) with the excitation light at each absorption maximum.

PL lifetime decay curves

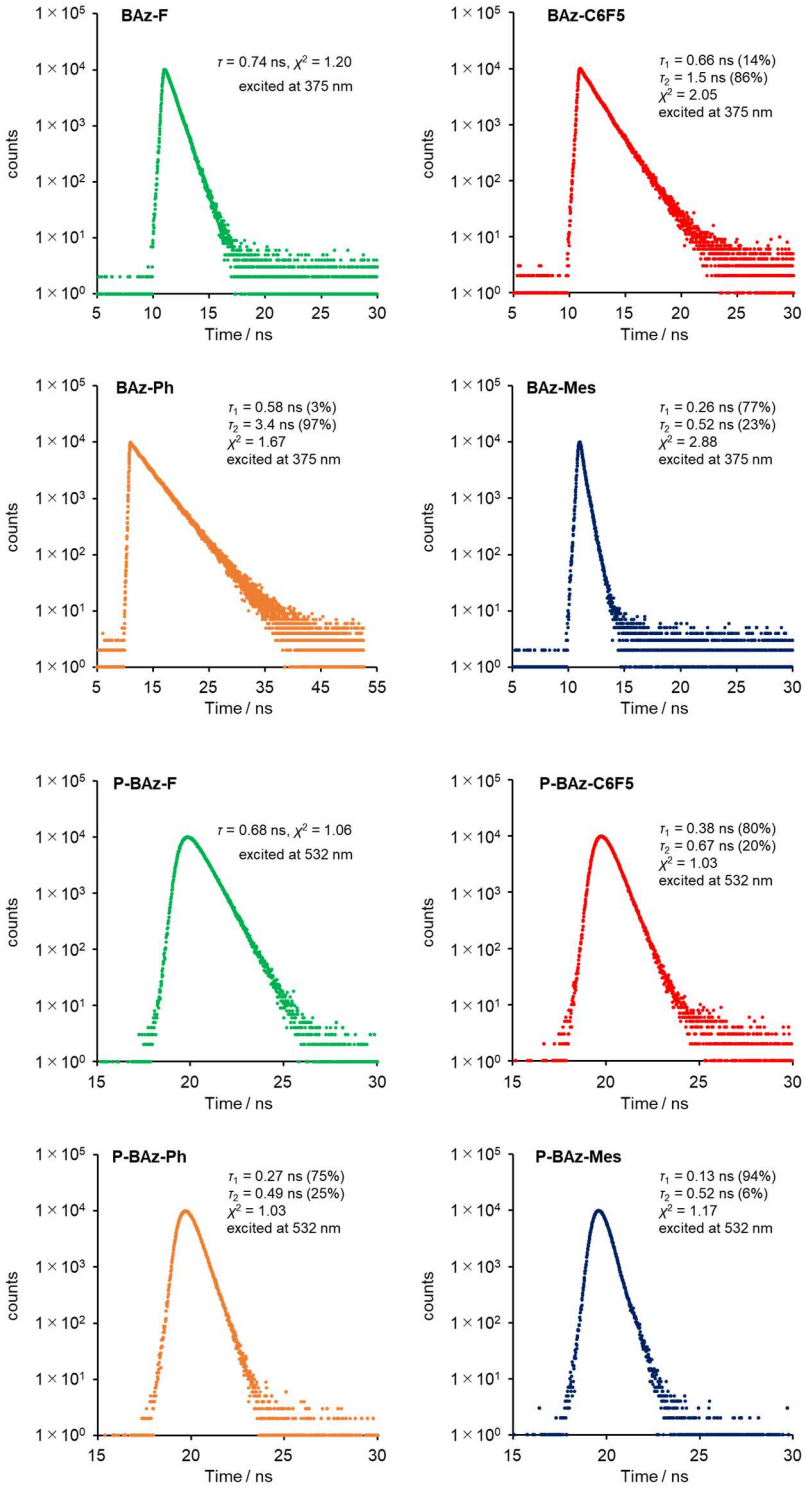

Figure S3. PL lifetime decay curves of **BAz** complexes in solid state and polymers in toluene (1.0×10^{-5} M) at room temperature (excited at 375 nm with a LED laser, and 532 nm with a LED). Their emissions at the PL peak tops were monitored.

Computational details for theoretical calculation

The Gaussian 16 program package[4] was used for computation. We optimized the structures of the **BAz-F**, **BAz-C6F5**, **BAz-Ph**, **BAz-Mes**, **BAz-F-BT**, **BAz-C6F5-BT**, **BAz-Ph-BT** and **BAz-Mes-BT**, in the ground S_0 states and calculated their molecular orbitals. The DFT was applied for the optimization of the structures in the S_0 states at B3LYP/6-311G(d,p) level. We calculated the energy of the transitions with optimized geometries in the S_0 states by time-dependent (TD) DFT at B3LYP/6-311G(d,p) level. The structure of model compounds, **BAz-F-BT**, **BAz-C6F5-BT**, **BAz-Ph-BT** and **BAz-Mes-BT**, are shown below.

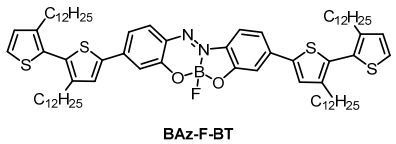

BAz-F-BT

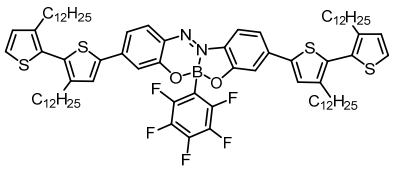

BAz-C6F5-BT

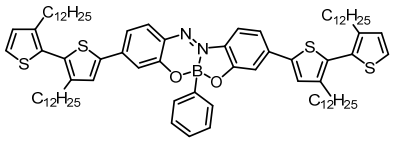

BAz-Ph-BT

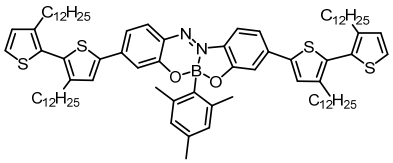

BAz-Mes-BT

Table S1. Results of representative transitions of **BAz** complexes from TD-DFT calculations

	Energy gap / eV	**Wavelength / nm**	**Oscillator Strength**	**transition**	**Assignment (Weight) (Contribution)**
BAz-F	2.6788	462.83	0.5457	$S_0 \rightarrow S_1$	HOMO → LUMO (0.68044) (93%)
					HOMO−1 → LUMO (0.11833) (3%)
					HOMO−2 → LUMO (0.13842) (4%)
BAz-C6F5	2.5302	490.01	0.4124	$S_0 \rightarrow S_1$	HOMO → LUMO (0.68307) (93%)
					HOMO−3 → LUMO (0.17437) (6%)
BAz-Ph	2.4165	513.06	0.2648	$S_0 \rightarrow S_1$	HOMO → LUMO (0.65456) (86%)
					HOMO−1 → LUMO (−0.22580) (10%)
					HOMO−4 → LUMO (−0.11410) (3%)
BAz-Mes	2.0327	609.96	0.0170	$S_0 \rightarrow S_1$	HOMO → LUMO (0.68373) (93%)
					HOMO−2 → LUMO (−0.16578) (5%)
	2.1617	573.56	0.0038	$S_0 \rightarrow S_2$	HOMO−1 → LUMO (0.69254) (96%)
					HOMO−2 → LUMO (0.11108) (2%)
	2.4273	510.79	0.3108	$S_0 \rightarrow S_3$	HOMO → LUMO (0.14603) (4%)
					HOMO−1 → LUMO (−0.12091) (3%)
					HOMO−2 → LUMO (0.65809) (87%)
					HOMO−4 → LUMO (−0.15645) (5%)
BAz-F-BT	2.1932	565.31	1.5942	$S_0 \rightarrow S_1$	HOMO → LUMO (0.70518) (99%)
BAz-C6F5-BT	2.1230	584.01	1.4616	$S_0 \rightarrow S_1$	HOMO → LUMO (0.70480) (99%)
BAz-Ph-BT	2.1366	580.29	1.3138	$S_0 \rightarrow S_1$	HOMO → LUMO (0.69877) (98%)
BAz-Mes-BT	2.0531	603.90	0.4690	$S_0 \rightarrow S_1$	HOMO → LUMO (0.52321) (55%)
					HOMO−1 → LUMO (0.45475) (41%)
					HOMO−2 → LUMO (−0.12277) (3%)
	2.1542	575.54	0.7715	$S_0 \rightarrow S_2$	HOMO → LUMO (−0.45801) (42%)
					HOMO−1 → LUMO (0.52518) (55%)

Molecular orbitals of BAz complexes

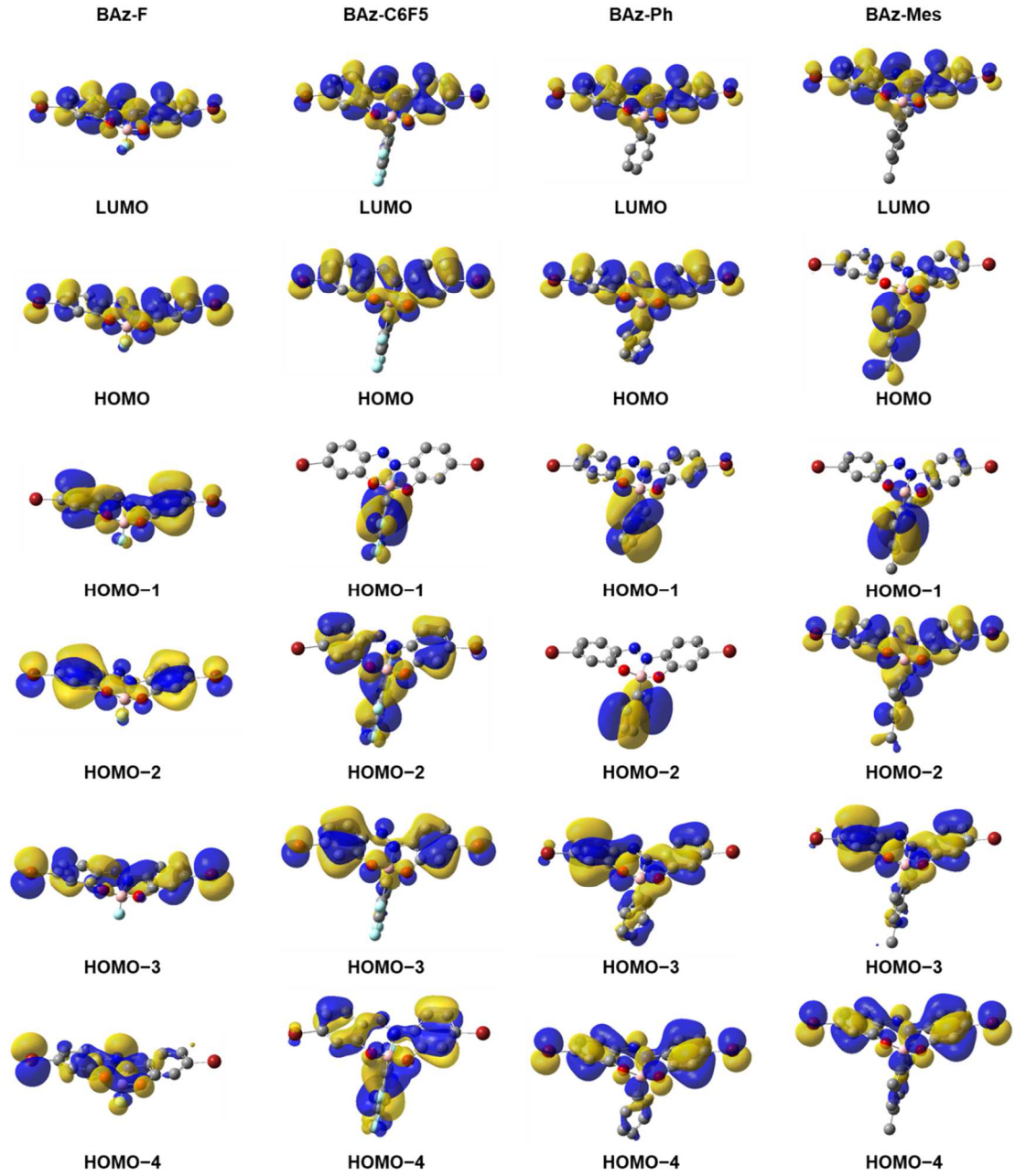

Figure S4. Selected Kohn–Sham orbitals of **BAz** complexes obtained with DFT calculations (isovalue = 0.02). Hydrogens were omitted for clarity.

Selected Kohn–Sham orbitals of model compounds

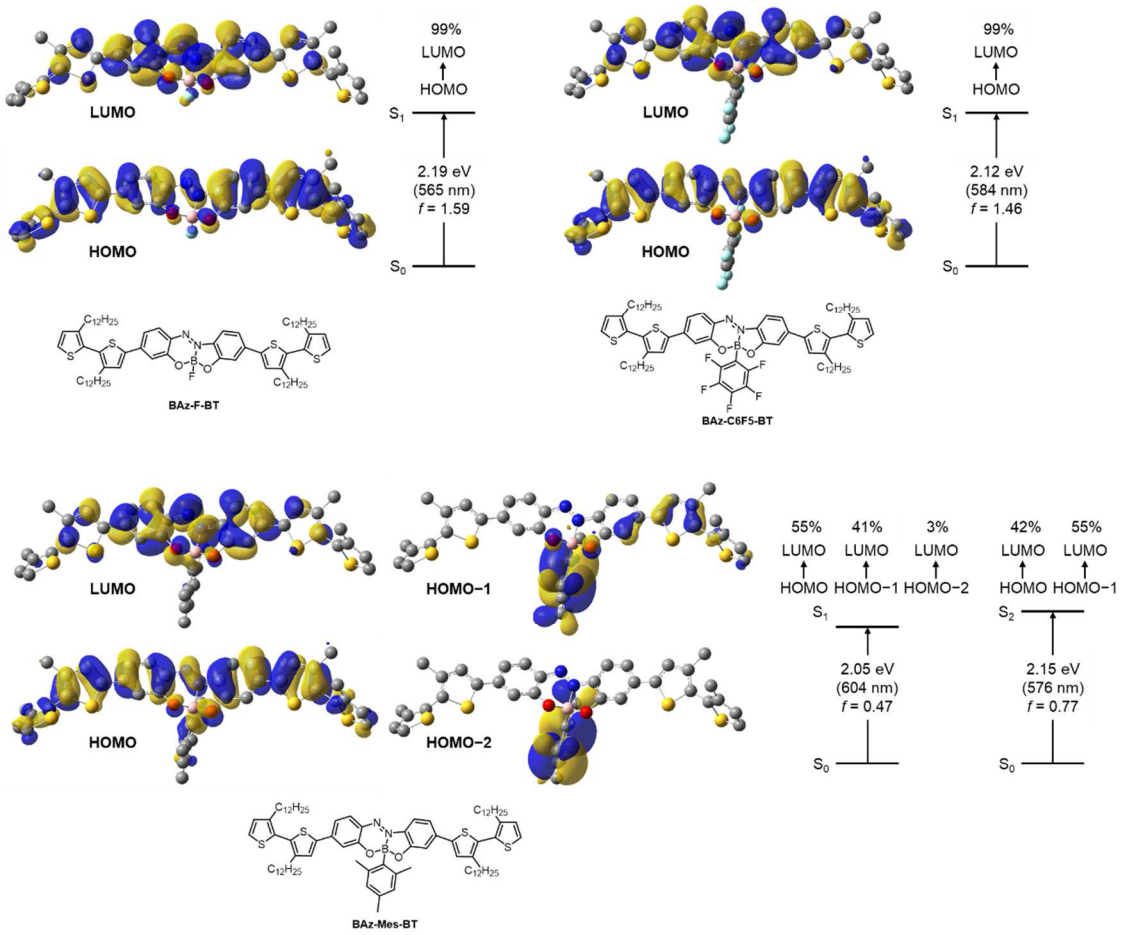

Figure S5. Selected Kohn–Sham orbitals of model compounds **BAz-F-BT**, **BAz-C6F5-BT** and **BAz-Mes-BT** main transition band and contributed MOs with rate of contribution (*f*: oscillator strength) obtained with DFT or TD-DFT calculations (isovalue = 0.02). Hydrogens were omitted for clarity.

References

[1] M. Gon, K. Tanaka and Y. Chujo, *Angew. Chem. Int. Ed*. **2018**, *57*, 6546.

[2] R. Yoshii, K. Tanaka, Y. Chujo, *Macromolecules* **2014**, *47*, 2268.

[3] X. Guo, Q. Liao, E. F. Manley, Z. Wu, Y. Wang, W. Wang, T. Yang, Y.-E. Shin, X. Cheng, Y. Liang, L. X. Chen, K.-J. Baeg, T. J. Marks and X. Guo, *Chem. Mater*. **2016**, *28*, 2449.

[4] Gaussian 16, Revision A.03, M. J. Frisch, G. W. Trucks, H. B. Schlegel, G. E. Scuseria, M. A. Robb, J. R. Cheeseman, G. Scalmani, V. Barone, G. A. Petersson, H. Nakatsuji, X. Li, M. Caricato, A. V. Marenich, J. Bloino, B. G. Janesko, R. Gomperts, B. Mennucci, H. P. Hratchian, J. V. Ortiz, A. F. Izmaylov, J. L. Sonnenberg, D. Williams-Young, F. Ding, F. Lipparini, F. Egidi, J. Goings, B. Peng, A. Petrone, T. Henderson, D. Ranasinghe, V. G. Zakrzewski, J. Gao, N. Rega, G. Zheng, W. Liang, M. Hada, M. Ehara, K. Toyota, R. Fukuda, J. Hasegawa, M. Ishida, T. Nakajima, Y. Honda, O. Kitao, H. Nakai, T. Vreven, K. Throssell, J. A. Montgomery, Jr., J. E. Peralta, F. Ogliaro, M. J. Bearpark, J. J. Heyd, E. N. Brothers, K. N. Kudin, V. N. Staroverov, T. A. Keith, R. Kobayashi, J. Normand, K. Raghavachari, A. P. Rendell, J. C. Burant, S. S. Iyengar, J. Tomasi, M. Cossi, J. M. Millam, M. Klene, C. Adamo, R. Cammi, J. W. Ochterski, R. L. Martin, K. Morokuma, O. Farkas, J. B. Foresman, and D. J. Fox, Gaussian, Inc., Wallingford CT, 2016.